

Dear Alex Iezzi,

thank you very much for taking the time and interest to deliver this very thorough and constructive review of our manuscript. We carefully studied your comments and made changes and corrections to the manuscript where necessary. We hope our changes and corrections are sufficient to make our article suitable for publication soon. Your comments and suggestions certainly helped to improve quality and clarity of the paper.

Thank you again, best regards

Christoph Pilger and co-authors

RESPONSES to Reviewer 2 (provided below each reviewer comment in green):

Specific Comments:

Line 28:

Do you use time-dependent attenuation and/or propagation modeling in this paper? Or are you referring to using atmospheric conditions close to the earthquake origin time since atmospheric conditions can change over short time scales? If not, please omit this phrase. If so, please add text to the manuscript describing your time-dependent propagation modeling.

RESPONSE: According to the reviewer's suggestion we omit the phrase time-dependent. It is a reference to the atmospheric conditions close to the earthquake origin time, yes, but not a reference to time-dependent modeling, which we do not perform.

Lines 49-51:

Can you provide a reference for this statement?

RESPONSE: The reference would be the USGS archive of earthquakes related to the Sulawesi one, as stated in the data availability section in the end of the paper. We rephrased the sentence to mention the USGS Sulawesi earthquake event page as a literature reference, also quantifying the number of related events described in these lines.

Line 52:

It may be beneficial to add an inset to Figure 1 with a zoom in on the source region that shows the city and rupture zone in more detail that can be pointed to in the introduction.

RESPONSE: Instead of an inset, a second subfigure was added to figure 1, zooming in on the source region and showing the rupture zone as well as the city of Palu. The figure caption was changed accordingly.

Line 79 (and in general):

There seems to be a variety of terms to describe different sources of infrasound (e.g. epicentral, seismoacoustic waves, secondary, etc). I suggest either condensing your definitions to distinguish between epicentral infrasound and secondary infrasound, or explicitly stating how the terms differ in the manuscript.

RESPONSE: According to the remarks of both reviewers for a harmonized use and definition of the two concepts of infrasound sources studied here, we modified the whole manuscript (see extended comment to reviewer1's similar remark) and keep with either "epicentral infrasound" or "seismoacoustic". We removed the other terms.

Lines 100-101:

This is more of a personal preference that you don't have to follow, but it may help highlight your results if instead of starting sentences off with "Figure XX shows", sentences start by stating what the figure shows as the subject of the sentence. For example,

"Figure 1 shows the earthquake epicenter as well as the nearest stations around the event."

Could be changed to

"The earthquake epicenter, as well as the nearest infrasound stations around the event, is shown in Figure 1"

RESPONSE: We agree with the reviewer's suggestion and changed the phrase accordingly. We also checked and modified the manuscript regarding further phrases like "figure xx shows".

Line 101:

It could be beneficial to give a quick mention of the ranges here, as done in Line 23.

RESPONSE: Distances were added according to the reviewer's suggestion.

Line 102:

You can mention that the detection/no detection you describe in this paragraph will be shown in the analysis of section 3.

RESPONSE: references to section 3 were added according to the reviewer's suggestion.

Lines 105-106:

Did you check other IMS arrays? If not, it may be best to refrain from making this assertion.

RESPONSE: Yes, we checked other more remote IMS arrays for signals from the 28 September 2018 Sulawesi earthquake and found no indications related to this event.

Line 107:

I know SING is only a single sensor and therefore array processing cannot be performed, but I would suggest adding a figure of the waveform somewhere since it is mentioned it a few times.

This can be done as part of figure 2, on its own in the main text, or in supplemental material.

RESPONSE: A SING signal plot and an INFERNO analysis of it is added to the supplement, both giving a representation of the SING station data and the INFERNO method mentioned in the manuscript. Manuscript text now refers to the supplementary figure in two adequate passages.

Line 119:

This may be a good place to define apparent velocity and state why it is useful (indicates arrival

inclination which can be used to infer propagation path, i.e. higher trace velocity likely indicates arrivals from higher altitude ducts).

RESPONSE: We added explanations to back-azimuth and apparent velocity and their use to derive direction and inclination of signal arrivals.

122-123:

It could be good to reference Matoza et al (2017) here.

Matoza, R. S., D. N. Green, A. Le Pichon, P. M. Shearer, D. Fee, P. Mialle, and L. Ceranna (2017), Automated detection and cataloging of global explosive volcanism using the International Monitoring System infrasound network, *J. Geophys. Res. Solid Earth*, 122, 2946–2971, doi:10.1002/2016JB013356.

RESPONSE: Agreed. Reference was added to manuscript and literature.

Line 124:

I suggest being more specific and stating propagation path. Also, “identified” might be a strong word especially at such long distances with uncertainties in the windfiles, possibly “inferred” or “plausible” would be better words? It may also be useful to describe celerity here, as I would argue it is usually a much more decisive propagation path indicator than trace velocity or frequency content (when the origin time of the event is known).

RESPONSE: we stated propagation “path” and changed “identified” to “inferred”, according to the reviewer’s suggestion. We do not describe celerity here, since the paragraph is a description of PMCC derived parameters and the information from them. To use celerity, specific source information is needed to calculate traveltime and distance and derive celerity from it. Celerity will be described in more detail later on according to Reviewer1’s Specific comment #6.

Line 128:

I suggest qualifying this sentence to station that the attenuation map is that of the surface (where the arrays are). This is important because you map stratospheric wind vectors on the same plot and not all readers may infer this.

RESPONSE: clarification was made according to the reviewer’s comment by adding “at surface level” to the given line.

Lines 144-147:

For merging the lower atmospheric ECMWF files with upper atmospheric climatologies, did you use Doug Drob’s G2S model? If so, this should be explicitly stated and Drob et al (2003) should be cited.

RESPONSE: No, Doug Drob’s model G2S is not used, but a self-constructed merging approach of the authors of this study.

Lines 148-158:

I believe this methodology does not account for atmospheric variability (which caused location biases in the Shani-Kadmiel et al (2017) paper). Please specify either way in the manuscript here or in the discussion section.

RESPONSE: A statement of the method not accounting for atmospheric variability and thus introducing location biases in addition to the measurement uncertainty and the bias by using a fixed celerity was added to the second paragraph of the discussion. The method nevertheless proves to provide realistic estimates since the averaged conditions used (300 m/s stratospheric ducted signal) are quite near to the ones calculated from observations at the three nearest stations (stated in the text).

Lines 161 – 165:

Please state your filter bands used in the manuscript text (it is only stated in the figure caption)

RESPONSE: we added the filter bands used in the manuscript text.

Line 165:

It may be good to mention back-azimuth here as that is the term that is used in the rest of the paper

“direction of origin (back-azimuth)”

RESPONSE: we modified the phrase according to the reviewer’s suggestion. A definition/explanation of back-azimuth was already given in response to a previous comment (related to line 119 above).

Lines 166:

I assume you mean 4 infrasound arrays that made detections?

RESPONSE: Yes, “infrasound” was added in the text.

Line 168:

Celerity should be defined earlier (see comment for line124). Also, a more precise definition of celerity would be “the horizontal distance between source and receiver divided by the total travelttime”.

RESPONSE: Corresponding to our statement for line 124, we do not define celerity before and mention it here for the first time. In agreement with reviewer1’s specific comment #6, we provide a more precise definition of celerity here following the reviewers’ suggestions.

Table 1:

The expected arrival time row may not be necessary, as it requires the assumption of a stratospheric celerity (0.3 km/s), which is not always the correct propagation path.

Also, please state in the text how is signal duration defined.

RESPONSE: expected arrival times may not be correct if the celerity is different from 300. Nevertheless it is by definition (“expected”) an assumption and helps the reader and the discussion in the text to compare observations to expectations, so we keep the row. A definition of the use of

signal duration (“derived from the width of the high-frequency part signals originating from epicentral directions in the PMCC analyses”) is added to the manuscript text.

Figure 2:

Adding subplot labels (a, b, c) that can be referred to in the results section may help support your claims and help the reader follow along.

The font sizes might be slightly small in this figure.

RESPONSE: Subplot labels (a-d) were added to figure 2, according to both reviewers' remarks. Label font sizes were slightly increased, but a larger increase is difficult since the figure is already quite dense. See reply to reviewer 1 for further details.

Line 188:

The list format of your results section is a bit odd. I suggest removing this line and making the bullets into paragraphs.

RESPONSE: This part of the manuscript was modified according to the reviewer's suggestion.

Line 202:

It might be nice to add a plot of the winds as supplemental material (even if it is just one sonde above the source) and discuss if the back azimuth deviations are consistent with the cross winds of the specified propagation duct.

RESPONSE: A multiple plot of the crosswind situation is added to the supplement for each of the four stations and a profile along the source to the station. It should allow insights on the crosswind situation and possible resulting backazimuth deviations along the complete signal propagation path. Nevertheless the situation is not that clear and simple (so that a single crosswind plot above the source could not provide a realistic representation), since atmospheric profiles, also those of the crosswind, change with range and altitude. It is not clear and easy to say which altitude parts influence the signals most and lead to back-azimuth variations. Some considerations are added to the caption, but they cannot cover the whole picture of a changing atmosphere along thousands of kilometers. It can be reconsidered if this additional picture is worth to be shown. The complementary figure is referenced in the given paragraph (from line 202) where back-azimuth deviations are mentioned.

Line 241:

This sentence is unnecessary and could be removed.

RESPONSE: Agreed, the sentence was removed from the manuscript.

Line 243:

Please clarify the phrase “acoustic velocities”. Do you mean apparent velocity?

RESPONSE: Yes, “apparent” was added to the text.

Line 244:

It should be qualified that celerities outside these bounds exclude purely acoustic waves from the origin at the time of rupture.

RESPONSE: We modified the phrase highlighting origin and rupture time, according to the reviewer's suggestions.

Lines 260-265:

Please be more clear on your definitions of both attenuation and propagation modeling. You calculate them using different methods, but they both show results of transmission loss with your attenuation shown in map view and the propagation modeling shown as a cross section.

RESPONSE: According to the comments of both reviewer's we streamlined the language around the concept of transmission loss and skipped the misleading use of "attenuation modeling". We thus define the semi-empirical technique for transmission loss calculations (fig3) as the first technique used, its description modified in various text passages. We keep the concept of propagation modeling (fig4) as a second technique and clarified the differences and benefits of those two concepts both applied in the study. Lines 260-265 are modified to: "Transmission loss calculations using firstly a semi-empirical method for a horizontal representation (map view, figure 3) and secondly a parabolic-equation-based propagation model for a vertical representation (cross section, figure 4) are performed...".

Line 268:

What is the spatial resolution of the range dependent atmospheric profiles? 0.5 x 0.5 degree as stated in Figure 3 caption? Please state this in the manuscript text.

RESPONSE: the 0.5° x 0.5° resolution from the figure caption is also added to the manuscript text here.

Line 270:

Please elaborate on what INFERNO is and how you use it.

RESPONSE: The INFERNO software, its key features and its application within this study is elaborated in more detail in the given passage, following the recommendation of both reviewers.

Lines 266-295:

The transmission losses, associated uncertainties for each array, and source frequency in this paragraph could all be put into a table to more concise and easily get your point across to the reader.

RESPONSE: A table was added according to the reviewer's suggestion and the according manuscript text was modified; the numbers were shifted to the table and the text was shortened to just give ranges of transmission loss values and uncertainties.

Figure 4:

Why did you choose 1Hz modeling? That seems a bit high for propagation of such large distances.

RESPONSE: This is true, but 1 Hz is a compromise between the 0.2 Hz (figure 3a) of the low-frequency acoustic energy maximum and the 3 Hz (figure 3b) of the high-frequency signal content which is unique for the stratospheric ducted signal parts. It is also a matter of necessity to be able to present the stratospheric ducts in a clear and concise figure. When going to lower frequencies, there is less attenuation and higher wavelengths and the modeling as well as picture becomes less detailed and more blurred, losing the clear optical representation of the stratospheric waveguides which are the main message of the figure.

Figure 5:

Lines 384-395 refer to Sulawesi Island, North Maluku, etc. It might be helpful to label these areas in the figure so the reader can more easily follow along. Or, if you chose to add an inset to Figure 1 you can refer to the locations there.

RESPONSE: References to island names were added as labels to figure 1 and 5, instead on an inset, a second subfigure is added to figure 1 (see separate comment).

Line 425:

Tiny semantic issue, but I don't believe the earthquake is named after the mountain. The earthquake ruptured the Denali fault as well as the Toschunda fault and is located in/near Denali National Park.

RESPONSE: Good to know, we changed the mountain association to the fault one.

Line 449:

Do you have a reference for this?

RESPONSE: Unfortunately not. To my knowledge there was no infrasound study about these events yet, so the statements "are estimations following data analyses performed by authors of this study" (this is already mentioned in the manuscript).

Line 463:

I would argue that both topography and conducive propagation conditions are necessary for detection.

RESPONSE: Yes, the "conductive propagation conditions" are added to the end of the paragraph, where station detection and not source characteristics are described.

Technical Corrections:

Line 25

"is supposed to" sounds a bit awkward

Perhaps "The seismic-to-acoustic coupling at nearby terrain features *is shown to* generate distinct infrasonic signatures clearly recordable at remote infrasound arrays.

RESPONSE: instead of a correction of the wording the complete sentence was omitted since it is more or less redundant to the rest of the abstract and critical in the context of the reviewer1 nomenclature harmonization comment (also reviewer2 comment to line 79 and in general).

Line 27:

Suggest adding the word “infrasound” for clarity.
Event-related *infrasound* observations

RESPONSE: the phrase was modified according to the reviewer’s suggestion.

Lines 30, 95, 148, 358:

In these lines, “back tracking” is used. Please choose one term (I think “back projection” is the most widely used) and use throughout the manuscript.

RESPONSE: the nomenclature was modified to a homogenized use of “back projection” throughout the manuscript according to both reviewers’ suggestions.

Line 41:

Do you mean “a very high *rate of* natural seismicity”?

RESPONSE: the phrase was modified according to the reviewer’s suggestion.

Line 63:

“in the course of” may better be stated as “surrounding this event”

RESPONSE: the phrase was modified according to the reviewer’s suggestion.

Line 65:

Would it be more appropriate to say “both” instead of “either”?

RESPONSE: the phrase was modified according to the reviewer’s suggestion.

Line 179:

I don’t think “from above” is necessary.

RESPONSE: the phrase was skipped according to the reviewer’s suggestion.

Line 196:

There should be a better way to cite this. Please check the NHESS citation guidelines.

RESPONSE: there is a USGS event page to the Sulawesi 2018 earthquake, which we referenced according to the reviewer’s suggestion.

Figure 3:

The stratospheric wind vectors pretty hard to see. Can you make them slightly larger

RESPONSE: Arrow length and arrow head size of stratospheric wind vectors in figure 3 were enlarged according to the reviewer's suggestion.

1 **Infrasound and seismoacoustic signatures of the 28 September ~~28th~~-2018 Sulawesi super shear**
2 **earthquake**

3
4
5 Christoph Pilger¹, Peter Gaebler¹, Lars Ceranna¹, Alexis Le Pichon², Julien Vergoz², Anna Perttu³,
6 Dorianne Tailpied³, Benoit Taisne³

7
8 1 – BGR (Federal Institute for Geosciences and Natural Resources), Hannover, Germany
9 2 – CEA, DAM, DIF, 91297 Arpajon, France
10 3 – EOS / NTU (Earth Observatory of Singapore / Nanyang Technological University), Singapore

11
12 Corresponding author: Christoph Pilger; BGR, Hannover, Germany; christoph.pilger@bgr.de

13
14 **Abstract**

15 A magnitude 7.5 earthquake occurred on 28 September ~~28th~~-2018 at 10:02:43 UTC near the city of Palu
16 on the Indonesian island of Sulawesi. It was a shallow, strike-slip earthquake with ~~fractures up to the~~
17 ~~surface and~~ a rupture extending to length of about 150 km and reaching the surface. Moreover, this
18 earthquake was identified as one of very few events having a super shear rupture speed.

19 Clear and long-lasting infrasound signatures related to this event were observed by four infrasound
20 arrays of the International Monitoring System of the Comprehensive Nuclear-Test-Ban Treaty
21 Organization as well as by one national infrasound station in Singapore. Although these infrasound
22 stations SING (Singapore), I39PW (Palau), I07AU (Australia), I40PG (Papua New Guinea) and I30JP
23 (Japan) are located in large distances between 1800 km and 4500 km from the earthquake's epicentral
24 region, the observed infrasound signals associated to this event were intense, including both seismic
25 and acoustic arrivals. ~~The seismic-to-acoustic coupling at nearby terrain features is supposed to~~
26 ~~generate distinct infrasonic signatures clearly recordable at remote infrasound arrays.~~

27 A detailed study of the event-related infrasound observations and the potential infrasound generation
28 mechanisms is presented covering range-~~and time~~-dependent infrasound ~~attenuation-transmission~~
29 loss and propagation modeling, characterization of the atmospheric background conditions as well as
30 identification of the regions of seismoacoustic activity by applying a ~~backtracking-back projection~~
31 method from the infrasound receivers to potential source regions. ~~The~~is back-projection of infrasonic
32 arrivals allows to estimate that the main infrasound source region for the Sulawesi earthquake is
33 related to the extended rupture zone and the nearby topography. This estimation and the comparison
34 to other super shear as well as large regional earthquakes identifies no clear connection between the
35 earthquake's super shear nature and the strong infrasound emission.

36
37 **Keywords**

38 Infrasound; seismoacoustics; ~~attenuation~~; propagation modeling; Sulawesi; super shear; earthquake;
39

40 1. Introduction

41 Indonesia is located in a region with a very high rate of natural seismicity above a complex setting of
42 plate tectonics. Subduction zones of convergent plate boundaries in this region define the largest faults
43 of the Earth's crust, and the region of highest and most intense earthquake activity. In fact, some of
44 the strongest and most destructive earthquakes recorded during the last decades have occurred in
45 Indonesia, like the 2004 moment magnitude (Mw) 9.3 Sumatra-Andaman earthquake and various
46 other events with Mw larger than 8 (*Pailoplee, 2017*). These strong offshore events can often generate
47 large and devastating tsunamis. Additional crustal scale faults are also located on the Indonesian island
48 of Sulawesi, including the Palu-Koro fault transecting the Northern part of the island (*Katili, 1978*). The
49 Frequent seismic activity is associated to this fault was quantified using the United States Geological
50 Survey (USGS) nearby seismicity data link (USGS, 2018), resulting in at least 60 earthquakes larger than
51 magnitude 5 within the last 20 years and four events larger than magnitude 6 previous to the event
52 discussed in this study.

53 The 28 September 28th-2018 Sulawesi earthquake occurred at 10:02:43 UTC near the Indonesian city
54 of Palu on the island of Sulawesi. It was estimated by the United States Geological Survey (USGS) as a
55 Mw 7.5 strike slip earthquake (*USGS, 2018*) along the Palu-Koru fault with a hypocenter location of
56 0.256°S and 119.846°E and a depth of about 20 km. Modeling indicates that the majority of the slip
57 occurred shallow on the fault (above 10 km) with an offset of up to 7 m horizontal slip and a dip slip of
58 up to only 2 m (*Socquet et al., 2019*). The rupture zone of the event extended north-to-south over
59 roughly 150 km, along the fault and through the city of Palu, with a high rupture velocity of 4.1 km/s
60 in average. This indicates it to be a so called super shear event having rupture velocities higher
61 than the corresponding shear velocities (see Bao et al., 2019; Socquet et al., 2019). The phenomenon
62 is comparable to the acoustic sonic boom, an effect where the source travels faster than its emitted
63 waves. Analogous to acoustics the super shear rupture generates a shear wave mach cone, which may
64 cause enhanced ground motion and result in increased damage potential (Bernard and Baumont, 2005;
65 Doan and Gary, 2009). The Sulawesi earthquake resulted not only in intense ground shaking up to
66 "considerable damages" of Modified Mercalli Intensity IX, but also in liquefaction, landslides, and local
67 tsunamis within Palu bay (see *Heidarzadeh et al., 2019; Omira et al., 2019; Jamelot et al., 2019*). A large
68 number of precursory earthquakes as well as aftershocks happened in the course of occurred
69 surrounding this event.

70 The intense ground shaking of either both the epicentral region and the nearby topography
71 from nearby the Sulawesi earthquake resulted in strong and clearly observed infrasound signatures,
72 which are the focus of this study. Infrasound, which is the sub-audible part of acoustic waves below 20
73 Hz, is generated by a large number of natural and anthropogenic sources (e.g. see *Le Pichon et al.,*
74 *2010, 2019*) and can propagate over distances of thousands of kilometers with little attenuation to be
75 recorded at highly sensitive infrasound arrays. Many sources of either explosive or eruptive
76 characteristic, or those coming along with large mass movements can generate infrasound (e.g.
77 *Gibbons et al., 2015a; Pilger et al., 2018*), including earthquakes.

78 Reports on infrasound from earthquakes in the USA (*Mutschlecner and Whitaker, 2005*) as well as in
79 Peru, China and Chile (*Le Pichon et al., 2002, 2003, 2006*) indicate that the epicentral ground
80 movement generates infrasonic pressure waves. Further studies on the Mw 9.3 Sumatra-Andaman
81 earthquake (*Le Pichon et al., 2005*), the Mw 9.0 Tohoku earthquake (Walker et al., 2013) and on Italian
82 earthquakes (*Marchetti et al., 2016; Shani-Kadmiel et al., 2017; Hernandez et al., 2018*) also highlight
83 infrasound generated from tsunami waves hitting the coastline and from secondary phenomena like
84 remote ground motion of mountain chains or extended basin areas, and from tsunami waves hitting
85 the coastline. This secondary infrasound by remote ground motion is often called seismoacoustic

86 waves, since the seismic waves (longitudinal, shear or surface) generated by an earthquake propagate
87 to distant terrain features where the wave energy is partly converted to atmospheric acoustic waves
88 in the infrasound frequency range (e.g., see *Arrowsmith et al., 2010; Hedlin et al., 2012*).

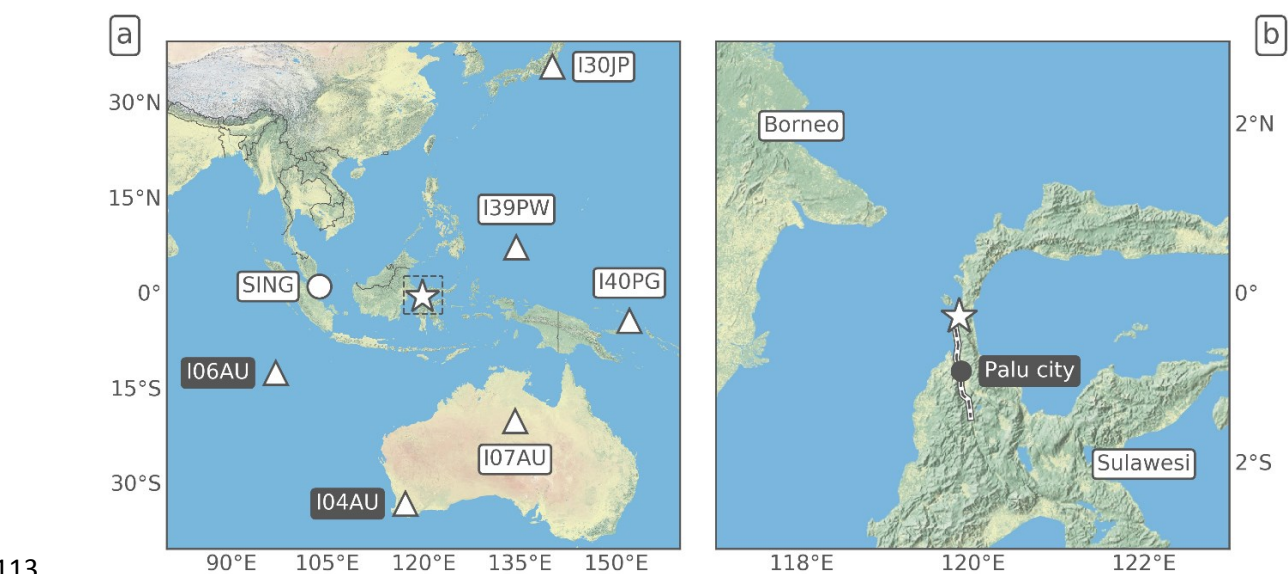
89 Although there ~~are many is quite a large number of~~ studies about infrasound generated by
90 earthquakes, only a small number of earthquakes with a super shear rupture speed have been
91 identified within the last 20 years (e.g. Izmit/Turkey in 1999, see *Bouchon et al., 2000*;
92 Kunlunshan/Tibet in 2001, see *Bouchon and Vallee, 2003*; Denali/Alaska in 2002, see *Dunham and*
93 *Archuleta, 2004*; Quinghai/China in 2010, see *Wang and Mori, 2012*; Craig/Alaska in 2013, see *Yue et*
94 *al., 2013*), and only one publication known to the authors identifies and investigates infrasound
95 observations ~~related to~~ a super shear earthquake, namely the Denali 2002 earthquake (*Olson et al,*
96 *2003*). Therefore, ~~one of the main tasks~~ a main objective of this paper is to investigate the potential of
97 a connection between super shear earthquakes and infrasound recordings of large amplitude.

98 This paper is structured as follows: Section 2 describes the data and methods applied within this study;
99 section 3 highlights the observations of epicentral infrasound and seismoacoustic signatures at remote
100 infrasound arrays; section 4 describes the modeling of infrasound ~~attenuation-transmission loss as well~~
101 ~~as~~ propagation and compares it to the observations; section 5 provides a ~~back-tracking~~ back
102 projection approach to identify the acoustic source regions of the observed signals and discusses the
103 event in comparison with similar earthquakes.

104

105 2. Data and Methods

106 This study mainly considers data recorded at infrasound arrays of the International Monitoring System
107 (IMS, e.g. described in *Le Pichon et al., 2010, 2019*) established under the Comprehensive Nuclear-
108 Test-Ban Treaty (CTBT). Data from various infrasound arrays of the International Monitoring System
109 (IMS) established under the Comprehensive Nuclear Test Ban Treaty (CTBT), are used within this
110 study. Figure 1 shows the earthquake epicenter as well as the nearest stations around the event. The
111 earthquake epicenter, as well as the nearest infrasound stations in distances between 1800 km and
112 4500 km around the event, are shown in figure 1.



114 *Fig 1: a) Map of the Sulawesi earthquake epicenter (star) and the locations of the nearest*
115 *surrounding infrasound stations (the circle corresponds to a single-sensor station, the triangles to multi-*

116 sensor IMS arrays; white-labeled stations registered the event, black-labeled ones did not). b) Zoom of
117 the epicentral source region showing in larger detail the rupture zone passing through the city of Palu.

118

119 The two IMS infrasound stations closest to the earthquake epicenter clearly registered the event
120 (I39PW in Palau and I07AU in Northern Australia, see section 3). Two further IMS stations at larger
121 distances found clear indications of signals related to the earthquake (I40PG in Papua New Guinea and
122 I30JP in Japan, also see section 3). However, two other Australian stations (I04AU and I06AU) as well
123 as all of the more distant IMS infrasound arrays recorded no signals related to the earthquake source.

124 Additional data from a single infrasound sensor in Singapore (SING) was investigated and also showed
125 signatures related to the earthquake (see figure S1 of the supplement). However, due to a lack of array
126 calculations and directional information by only a single sensor, no further studies are applied for this
127 data.

128 The PMCC method (Progressive Multi-Channel Correlation, see *Cansi, 1995*); used in this study is
129 available from the DTK-GPMCC application in the NDC-In-A-Box package. The main objective of the
130 NDC-In-A-Box project is to offer to all National Data Centers (NDCs) of CTBT member states the
131 capability to process and analyse seismic, infrasound and hydroacoustic data, and so to become active
132 contributors to the verification regime of the CTBT. Technically, it consists of a number of automatic
133 and interactive software tools which are packaged in a Virtual Machine distributed by the CTBT
134 International Data Center (IDC). Among this set of software, DTK-GPMCC is the interactive array
135 processing tool, it allows to configure and run the PMCC detector from waveforms of any technology,
136 and to display and analyze the results. PMCC is applied to the raw differential pressure recordings at
137 each of the IMS infrasound arrays' microbarometers to derive advanced data parameters like back-
138 azimuth, apparent velocity and frequency content of coherent signals thereby associated to different
139 events (see figure 2). Back-azimuth reflects the horizontal direction of signal origin, while apparent
140 velocity indicates the arrival inclination, where higher values correspond to propagation from higher
141 altitude ducts. Signals are identified as pixel information in distinct time steps and frequency bands
142 and are clustered to signal families related to the same event. 1/3 octave band configurations with an
143 inverse frequency distributed window length are implemented between 0.01 and 4.4 Hz (*Garces,*
144 *2013*). Signals can be associated to a certain source by e.g. applying cross bearing techniques on the
145 back-azimuth directions of two or more arrays (*Matoza et al., 2017*). The seismic or acoustic origin as
146 well as the propagation path of signals, e.g. ducting via stratosphere or thermosphere (*Drob et al.,*
147 *2003*), can be inferred from identified by the apparent velocity and frequency content of the
148 recordings.

149 In order to further investigate and understand the infrasound detection pattern in the region following
150 the Sulawesi earthquake, various simulations were performed to compute acoustic attenuation
151 transmission loss and to simulate infrasound propagation between the source and the stations.
152 Infrasound attenuationtransmission loss at surface level (see figure 3) was calculated using a
153 frequency-dependent, semi-empirical modeling technique coupled with realistic atmospheric
154 specifications along the infrasound propagation path (*Le Pichon et al., 2012; Tailpied et al., 2017*) in
155 order to draw a range- and frequency-dependent attenuation map estimating the acoustic pressure
156 loss between source and receivers in decibel (dB). The attenuation-transmission loss of the signal at
157 each station is associated to a confidence index that integrates uncertainties from the propagation
158 modeling and the atmospheric specifications. Infrasound propagation (see figure 4) was modeled using
159 a two-dimensional Parabolic Equation method (NCPA PAPE, see *Waxler et al., 2017*) to quantify and
160 visualize the ducting and as well as amplitude decrease between source and receivers.

161 ~~In both the semi-empirical and the parabolic equation-based transmission loss estimates,~~
162 ~~in both attenuation and propagation modeling,~~ data from the European Centre for Medium-range Weather
163 Forecast (ECMWF) meteorological model are used to derive the effective sound speed as the most
164 important background parameter for infrasound propagation. Indeed, this parameter, defined as
165 adiabatic sound speed modified by horizontal winds in the propagation direction of the modeled
166 sound, is used to provide the atmospheric background conditions along the propagation path between
167 the source and the stations (Wilson, 2003). Ducting along tropospheric, stratospheric or thermospheric
168 waveguides (Drob et al., 2003) can be estimated in the same manner as the total amplitude loss from
169 geometric spreading as well as atmospheric attenuation (Sutherland and Bass, 2004). ECMWF values
170 are used from 0 to 60 km altitude and merged with temperature and wind climatologies above
171 (MSISE00 and HWM07, see Picone et al., 2002, Drob et al., 2008) to provide seamless effective sound
172 speed profiles from 0 to 140 km altitude.

173 ~~Backtracking-Back projection~~ of the coherent earthquake-related signals observed at infrasound arrays
174 to their source region is performed within this study using a seismoacoustic method similar to that of
175 Marchetti et al. (2016) or Shani-Kadmiel et al. (2017), which is also part of the built-in capabilities of
176 PMCC (see figure 5). Assumed is a conversion of the initial seismic wave with crustal propagation
177 velocities of e.g. 4 km/s to acoustic waves with ~~an~~ average ~~celerities-speed~~ of e.g. 0.3 km/s at certain
178 terrain features, like steep or flat topography as e.g. mountain chains, islands, cliffs or extended plains.
179 This method identifies the seismoacoustic conversion areas and thus infrasonic source regions for the
180 signals observed, taking into account for each PMCC pixel the arrival time and back-azimuth direction
181 relative to a point source in space and time, here the Mw 7.5 earthquake epicenter. The cumulative
182 sum and frequency of occurrence of the ~~backtrackedprojected~~ origin locations therefore allows to
183 identify ~~seismoacoustic-infrasonic~~ source regions, either of epicentral or ~~secondary-seismoacoustic~~
184 origin.

185

186 3. Observations

187 The ~~28~~ September ~~28th~~-2018 Sulawesi earthquake was identified in the recordings of four IMS
188 infrasound arrays: I39PW, I07AU, I40PG and I30JP. Four to six hours of differential pressure recordings
189 from these stations following the earthquake origin time (10:02:43 UTC) are analyzed using the PMCC
190 method described in section 2. Signal parameters related to the earthquake are extracted from the
191 PMCC results in terms of arrival time and duration as well as direction of origin (~~back-azimuth~~) and
192 apparent signal velocity.

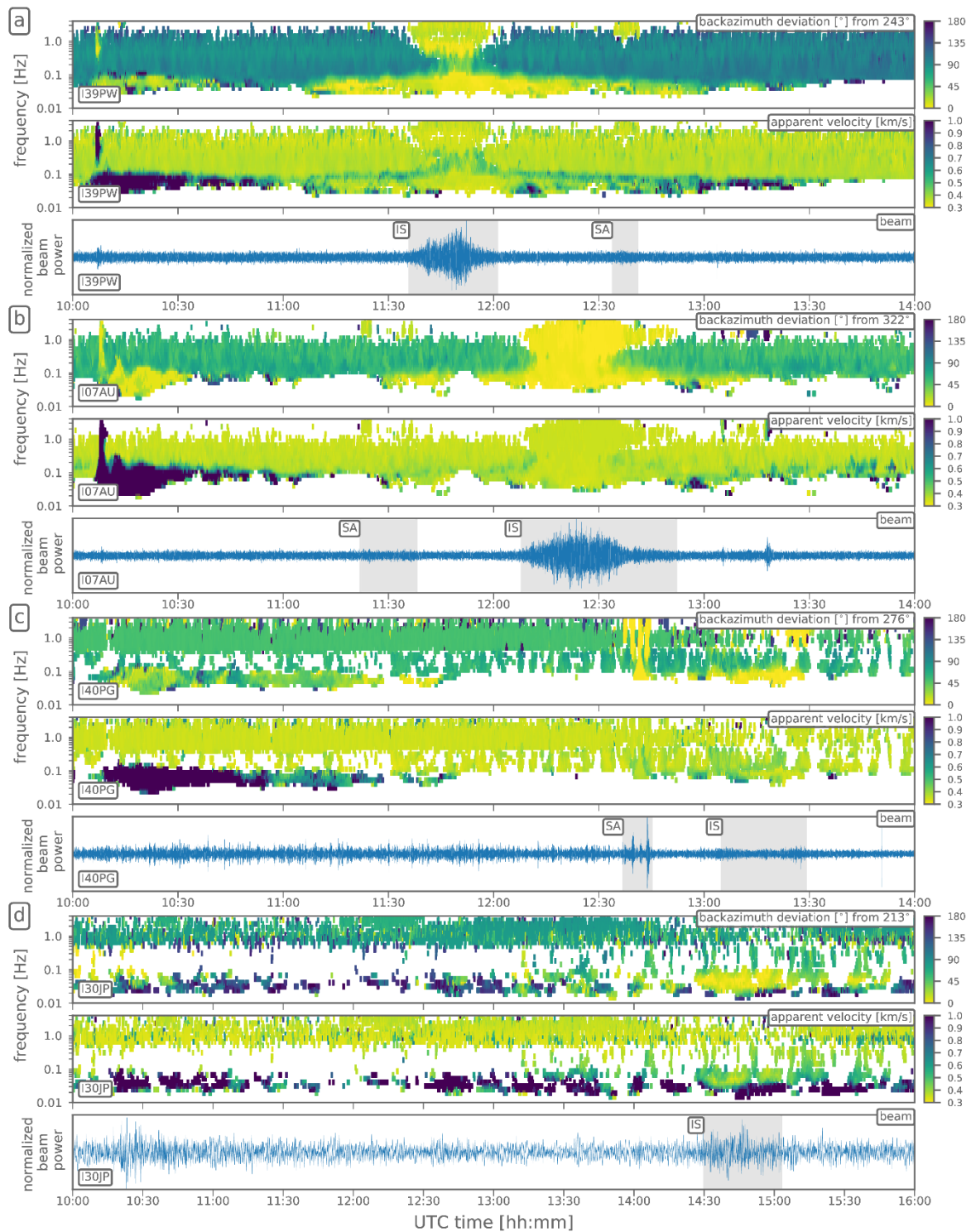
193 ~~Table 1 summarizes t~~These observations parameters for the four IMS ~~infrasound~~ arrays and for the
194 earthquake-related signal also identified in SING station data ~~are summarized in table 1~~. Furthermore,
195 source-to-station distances as well as expected back-azimuth directions and arrival times using a
196 celerity (~~epicentral distance divided by the traveltimespeed over ground~~) of 300 m/s are presented for
197 comparison. ~~Figure 2 provides a~~A graphical representation of ~~the waveform beams (bandpass-filtered~~
198 ~~between 0.6 and 4 Hz, except for I30JP, where it is 0.02 and 0.1 Hz) and the main PMCC findings -the~~
199 ~~main findings~~ for the four IMS stations ~~is provided in figure 2~~, highlighting epicentral infrasound arrivals
200 and their acoustic characteristics in the observations but also seismoacoustic and seismic signatures
201 related to the event.

202

203 Table 1: Findings from the observations of five infrasound stations and from theoretical distance-
 204 azimuth calculations to the Sulawesi epicenter. Main signal groups are labeled with "IS" (infrasound)
 205 and, secondary signals are labeled "SA" (seismoacoustic).

Station	SING	I39PW	I07AU	I40PG	I30JP
Distance to epicenter (km)	1788	1845	2689	3604	4474
Expected back-azimuth (°)	94	243	322	276	213
Expected 300 m/s arrival time (UTC)	11:42	11:45	12:32	13:23	14:11
Observed arrival time (UTC)	IS) 11:50	IS) 11:36 SA) 12:34	IS) 12:08 SA) 11:22	IS) 13:05 SA) 12:37	IS) 14:30
Observed signal duration (min)	IS) 10	IS) 25 SA) 7	IS) 44 SA) 16	IS) 24 SA) 8	IS) 33
Observed mean celerity (m/s)	IS) 267	IS) 290 SA) 200	IS) 304 SA) 514	IS) 309 SA) 380	IS) 263
Observed mean back-azimuth (°)	- (no array)	IS) 251 SA) 257	IS) 319 SA) 321	IS) 275 SA) 276	IS) 209
Observed mean apparent velocity (m/s)	- (no array)	IS) 383 SA) 359	IS) 356 SA) 371	IS) 351 SA) 360	IS) 436

206



207

208 Fig 2: Waveform beams and PMCC-derived results for the four infrasound arrays I39PW (a), I07AU (b),
 209 I40PG (c) and I30JP (d; stations are ordered sorted by epicentral distance from above, three frames per
 210 station, station labels in the lower left corners). Shown in the corresponding stations' top frames
 211 are the observed back-azimuth deviations from the direction to the earthquake epicenter (see labels in the
 212 upper right corners), in the middle frame the observed apparent velocities, and in the bottom frame
 213 the waveform beams. The whole 360° back-azimuth observations are converted to the given deviation
 214 plotting of $\pm 180^\circ$. Apparent velocities are saturated above 1 km/s. Beams are bandpass-filtered
 215 between 0.6 - 4 Hz and four hours of data are shown with the exception of I30JP where the beam is
 216 bandpass filtered between 0.02 - 0.1 Hz and six hours of data are shown. Main infrasonic (IS) and
 217 seismoacoustic (SA) signal groups (see table 1) are highlighted in grey.

219 ~~The main findings of the infrasound observations and PMCC analyses related to the earthquake are:~~

220 –Initial seismic waves with high-frequency components (0.3-3 Hz) are found in I39PW and I07AU data
 221 arriving four to six minutes after the origin time, indicating apparent P-wave velocities of 4-10 km/s,
 222 lasting about two minutes. These are followed by low-frequency (0.05-0.5 Hz), quasi-continuous
 223 seismic waves observed ~~in I39PW, I07AU, I40PG and possibly I30JP~~~~in all four arrays~~, likely related to
 224 seismic shear and surface waves, having velocities of 1-3 km/s. Aftershock activity as well as seismic
 225 signals from other regional earthquakes are also present in figure 2 for the hours after the main
 226 earthquake; aftershocks include 12 events of magnitude 5 or greater, and 40 events of magnitude 4 or
 227 greater within six hours following the event (~~source: USGS, 2018~~). Values for the arrival of seismic
 228 waves are not integrated in table 1, since the local ~~infrasound observations~~~~microbarometer output~~
 229 generated from ground-shaking of the sensors are not the focus of this study. Nevertheless, the
 230 infrasound sensors do work fairly well as seismic arrays ~~for this event~~~~here~~ (e.g. see *Gibbons et al.,*
 231 *2015b*) and the earthquake related seismic arrivals can clearly be identified in figure 2 having ~~back-~~
 232 ~~azimuths towards the epicenter and~~ apparent velocities exceeding 1 km/s (drawn with dark blue colors
 233 in the middle frame plot of each station indicating seismic and not acoustic signal speeds).

234 –Epicentral infrasound is clearly observed and produces the main signal with the largest waveform
 235 amplitudes in I39PW and I07AU (beams are plotted in figure 2 in the bottom frame plots of the
 236 respective stations, signals are highlighted by grey rectangles and “IS” labels). The analysis shows a
 237 broadband-frequency content (0.05 to 4.4 Hz) and long signal durations of 25 and 44 minutes ~~(derived~~
 238 ~~from the width of the high-frequency part signals originating from epicentral directions in the PMCC~~
 239 ~~analyses)~~. ~~Figure 2 emphasizes t~~~~These signals are emphasized in figure 2,~~ since the back-azimuth
 240 calculations as well as the ~~array beams~~~~beamforming~~ are focused ~~towardson the respective theoretical~~
 241 ~~back-azimuth for the earthquake~~ epicenter ~~calculated for each station~~ (yellow colors in the azimuth
 242 frame of each station indicating low to zero back-azimuth deviations from this ~~direction~~~~value~~). The low
 243 deviations from the theoretical back-azimuth directions (3° and 8°, see table 1 for the corresponding
 244 values) confirm the signals to be associated to either the epicenter, the rupture process at the surface
 245 or the ground shaking of topographic features on the island of Sulawesi. ~~Crosswinds, as shown in figure~~
 246 ~~S2 of the supplement, lead to certain back-azimuth deviations.~~ An azimuthal sweep is observed in the
 247 I07AU data from south to north (directions of 316° to 323°), consistent with the north-to-south rupture
 248 along 150 km. ~~Deviations from the expected backazimuth direction are largest in I39PW data (about~~
 249 ~~±10°)~~. The other ~~three~~ stations only show weak or no such ~~variations~~~~sweeps~~. ~~See figure S3 of the~~
 250 ~~supplement for a detailed representation of these findings using absolute backazimuth values.~~

251 –For the more distant stations I40PG and I30JP, the epicentral infrasound is consistent with the
 252 theoretical back-azimuths (1° and 4° deviation), but mostly allocated with frequencies below 0.1 Hz,
 253 indicating larger absorption of the high-frequencies along the long-distance propagation (see section
 254 4 for the corresponding propagation modeling). The high-frequency pulses in the I40PG recordings
 255 around 12:40 UTC are associated to a ~~secondary~~~~seismoacoustic~~ signal, which is discussed in the end
 256 of this section.

257 –In general, the observed back-azimuths fit very well to the theoretical ones calculated for the
 258 epicenter for all four stations, allowing the application of a cumulative back~~tracking~~ ~~projection~~
 259 method to locate the source regions of the observed infrasonic signals in section 5. The epicentral
 260 signals’ mean apparent velocities are all in the acoustic range valid for stratospheric propagation (350
 261 to 380 m/s, see table 1), with the exception of I30JP having higher mean apparent velocities of 436
 262 m/s. This together with low celerity values of 263 m/s and appearance of only low-frequency signals
 263 at this station strongly indicates thermospheric propagation for I30JP instead of stratospheric.

264 Thermospheric arrivals are expected to also be present in the other stations' observations apart from
265 the dominant stratospheric ones; their later arrival time and lack of high-frequency content
266 correspond to the long-lasting signal families following the main signal peak for many minutes in the
267 low frequencies. These signal families can be observed together with low-frequency seismic wave
268 activity and low frequency acoustic components from the stratospheric ducting in frequency bands
269 around 0.1 Hz. ~~They are~~ discernible only to a certain degree by the apparent velocities and arrival
270 times, being the slowest and latest arrivals from the epicenter. The celerities observed at I39PW, I07AU
271 and I40PG as well as the observed arrival times and signal durations well correspond to the expected
272 arrival times calculated using a 300 m/s celerity of average stratospheric propagation, quite close to
273 the actually observed values at I39PW, I07AU and I40PG (see table 1). The expected arrival times for
274 these stations are clearly within the main signals' observed time window and are only 2 to 6 minutes
275 shifted from the respective mid-point of the observed arrivals' time window (arrival time plus half of
276 the signal duration).

277 ~~—Microbaroms, which are infrasonic signals from interacting ocean surface waves (Donn and Naini,~~
278 ~~1973; Arduin and Herbers, 2013)~~ are also present in the recordings of I39PW and I07AU around 0.2
279 Hz and dominant before and after the earthquake signals, as well as surf or potentially anthropogenic
280 noise in I40PG and I30JP data around 1 Hz during the complete observation. These background (noise)
281 signals can clearly be separated, by back-azimuths (greenish colors in the top frame plots) from the
282 epicentral signal. ~~Infrasound signals can generally be distinguished from the seismic arrivals by their~~
283 ~~signal speed.~~

284 ~~—Secondary Seismoacoustic~~ signals are identified in I07AU, I39PW and I40PG data, coming from nearly
285 epicentral directions and having acoustic apparent velocities. They have high frequency content (above
286 1 Hz) and celerities below 200 or above 380 m/s, thus excluding purely acoustic waves propagating
287 from the epicenter at the time of the rupture, e.g. also those traveling through thermosphere or
288 troposphere. These ~~arrivals signals~~ could be seismoacoustic ~~arrivals precursors and successors~~ related
289 to the earthquake (their signal parameters are provided in table 1 and highlighted in figure 2 with the
290 label "SA"). A conversion of seismic to acoustic waves at certain, distinct terrain features might be
291 responsible for this kind of signals. Islands between Java and East Timor (south of Sulawesi) could be
292 the rough source region of the I07AU and I39PW signals, while islands of North Maluku (east of
293 Sulawesi) may be the source of the seismoacoustic signals in I40PG. Further details on back-
294 ~~tracking projecting~~ and thus identifying acoustic source regions are provided in section 5. Nevertheless,
295 from the given observations it is not possible to certainly confirm these ~~secondary~~ signal locations as
296 seismoacoustic source regions. None of the ~~secondary~~ signatures are observed at more than one
297 station and smaller groups of signals come from all regions around Sulawesi, also including neighboring
298 islands like Borneo. These signals are not necessarily associated to the earthquake, they could also
299 originate from other local infrasound or ambient noise sources and are just coincidental to the
300 earthquake in direction and timing. Alternatively, they and could be due to uncertainties in the array
301 processing or back ~~tracking projection~~ methods. ~~, or they are associated to other local infrasound or~~
302 ~~other noise sources and are just coincidental to the earthquake in direction and timing.~~

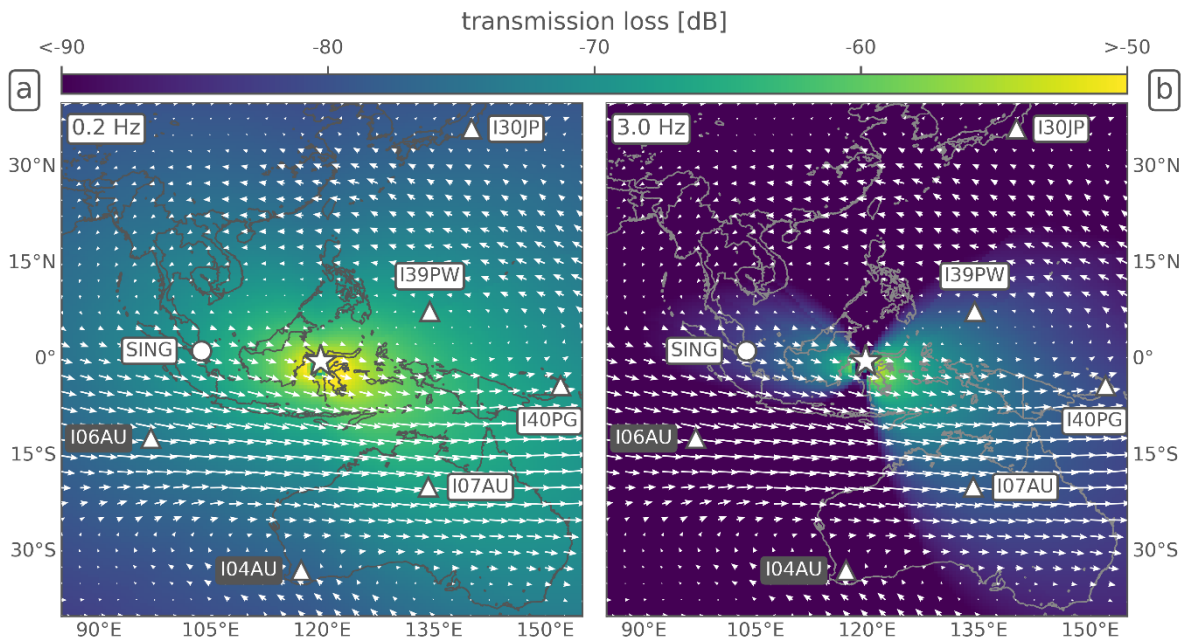
303

304 4. Modeling Results

305 ~~Attenuation and propagation modeling~~ Transmission loss calculations using firstly a semi-empirical
306 method for a horizontal representation (map view, figure 3) and secondly a parabolic-equation-based
307 propagation model for a vertical representation (cross section, figure 4) are performed in this section
308 to confirm and interpret the observed epicentral infrasound signatures as described above.
309 ~~Attenuation modeling~~ The semi-empirical method is used to estimate the frequency-dependent

310 transmission loss of a signal reaching the different infrasound stations, thereby characterizing its
 311 detectability. Propagation modeling is necessary to identify observed and expected signal arrivals, and
 312 to associate them to the prevailing atmospheric conditions between source and receivers and the
 313 corresponding ducting behavior.

314 ~~Figure 3 shows~~ The quantification of infrasonic transmission loss ~~is shown in figure 3 using the semi-~~
 315 ~~empirical method from atmospheric attenuation calculations~~ (see *Tailpied et al., 2017*) as well as a
 316 ~~representation~~ quantifying of the stratospheric wind field in terms of intensity and directionality.
 317 Simulations are performed within an 80° x 80° area ~~using 0.5° x 0.5° spatial resolution~~ around the
 318 earthquake epicenter for source frequencies of 0.2 Hz and 3 Hz. ~~At the low frequency of 0.2 Hz (figure~~
 319 ~~3a), where most of the acoustic energy is concentrated following calculations with the INFERNO~~
 320 ~~software (see Garces, 2013), the attenuation at all nearby infrasound stations is quite similar: values~~
 321 ~~in the map and their uncertainties are 66.8 ± 4.4 dB for I07AU, 67.3 ± 4.4 dB for I39PW, 69.0 ± 4.3 dB~~
 322 ~~for I40PG and 69.3 ± 4.3 dB for SING. Most of the acoustic energy is concentrated at the low frequency~~
 323 ~~band of 0.2 Hz. This was calculated applying the “The Infrasonic Energy, Nth Octave” (INFERNO)~~
 324 ~~algorithm (see Garces, 2013) to the station data. It calculates acoustic energy with frequency bands~~
 325 ~~based on the ANSI and ISO standards for noise characterization for the acoustic range extended into~~
 326 ~~the infrasound range, and it is based on fractional octave bands. An example is shown in figure S1 of~~
 327 ~~the supplement. Within this band the transmission loss calculated is similar for the closer stations SING,~~
 328 ~~I39PW, I07AU and I40PG (see figure 3a) and their values are between 66 dB and 70 dB with~~
 329 ~~uncertainties of about 4 dB (see table 2).~~ While values at these four stations indicate a northwest-to-
 330 southeast corridor of signal amplitudes in the same order of magnitude, the other stations in
 331 northeastern and southwestern directions have slightly higher ~~attenuation-transmission loss~~ values
 332 ~~of between~~ 73.7 ± 4.2 dB for I06AU, 77.3 ± 3.8 for I04AU and 79 dB (see table 2) 78.2 ± 4.0 for I30JP,
 333 indicating less favorable ducting conditions and detection probabilities at these stations.



334
 335 ~~Fig 3: Attenuation-m~~Map quantifying the acoustic ~~pressure-transmission~~ loss in dB (color-coded),
 336 calculated for (a) 0.2 Hz and (b) 3 Hz source frequencies on a 0.5° x 0.5° grid. Arrows show direction
 337 and intensity of the stratospheric wind field averaged between 30 and 60 km ~~altitude~~
 338 for the 28th of September 2018. The largest arrows represent a value of 25 m/s. For figure symbols and station labels
 339 see figure 1.

341 Table 2: Summary of transmission loss values and uncertainties (in dB), derived for all stations within
 342 this study from the frequency-dependent, semi-empirical method, as shown in figure 3.

	<u>SING</u>	<u>I39PW</u>	<u>I07AU</u>	<u>I40PG</u>	<u>I30JP</u>	<u>I06AU</u>	<u>I04AU</u>
<u>0.2 Hz</u>	<u>69.3 ± 4.3</u>	<u>67.3 ± 4.4</u>	<u>66.8 ± 4.4</u>	<u>69.0 ± 4.3</u>	<u>78.2 ± 4.0</u>	<u>73.7 ± 4.2</u>	<u>77.3 ± 3.8</u>
<u>3.0 Hz</u>	<u>84.1±24.2</u>	<u>79.7±21.4</u>	<u>78.3±17.9</u>	<u>81.0±13.7</u>	<u>107.0±32.1</u>	<u>101.4±26.6</u>	<u>118.7±34.9</u>

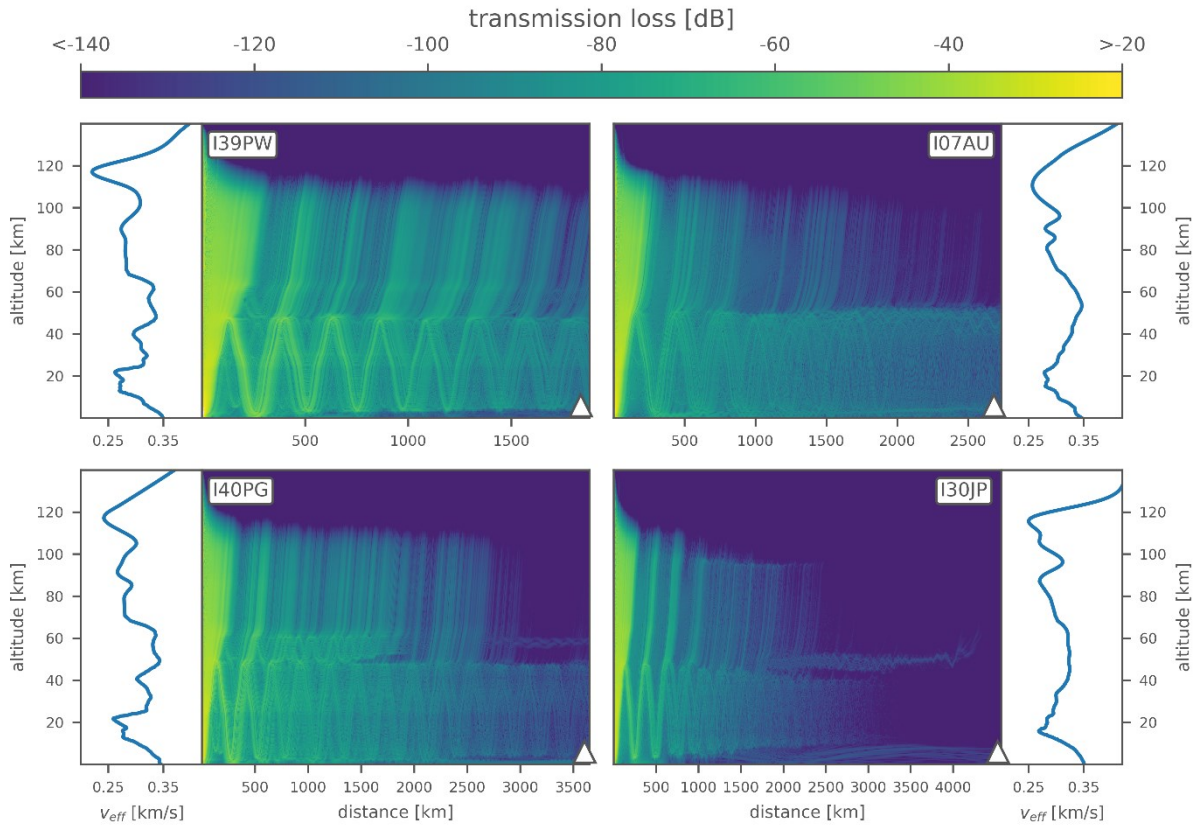
343
 344 The similarity of the ~~attenuation-transmission loss~~ values is consistent with the fact that low frequency
 345 signals are less affected by propagation effects along the path. Drawing the same picture with a source
 346 frequency of 3 Hz (figure 3b) indicates a different situation: station values for SING, I39PW, I07AU and
 347 I40PG now are between 78.3 ± 17.9 dB for I07AU, 79.7 ± 21.4 dB for I39PW, 81.0 ± 13.7 dB for I40PG
 348 and 84.1 ± 24.2 and 85 dB for SING with uncertainties of 13 to 25 dB (see table 2). These values are
 349 still quite similar to the ones estimated for 0.2 Hz, along the abovementioned corridor, although the
 350 uncertainties for the calculation are increased. The ~~attenuation-transmission loss~~ calculated from the
 351 epicentral source into all directions to a stronger degree visualizes for the high frequencies a focal
 352 effect in eastern and western directions with better observation conditions, while having regions with
 353 increased transmission loss attenuation regions and thus more unfavorable detection conditions in
 354 northern and southern directions. The ~~other~~ stations' values in these northern and southern directions
 355 are between 101.4 ± 26.6 dB for I06AU, 118.7 ± 34.9 for I04AU and 119 dB 107.0 ± 32.1 for I30JP with
 356 uncertainties of 26 to 35 dB, indicating remarkably higher ~~transmission lossattenuation~~ for these three
 357 stations due to propagation effects and atmospheric conditions and explaining, why no high-frequency
 358 signals (or signals at all) are observed at the respective stations.

359 Stratospheric wind conditions affect the propagation especially for the higher frequencies and point
 360 out the general possibility and effectiveness of a stratospheric duct. This is consistent with the fact that
 361 high frequency signals are more sensitive to the atmospheric conditions along the propagation path,
 362 also explaining the higher uncertainties in the calculation of these values. The stratospheric wind fields
 363 shown in figure 3 support this sensitivity by estimating the direction of the dominant stratospheric
 364 wind regime, which is eastward on the southern hemisphere's low latitudes, and the intensity of this
 365 30 to 60 km average, which is up to values of 25 m/s. Strong tailwinds thus support the stratospheric
 366 propagation to I07AU, while strong head- and crosswinds hamper it towards I04AU and I06AU. Winds
 367 are weaker from the source towards the other stations, mostly due to the equatorial wind situation of
 368 zonal stratospheric winds changing their direction here, rendering possible the simultaneous
 369 propagation in western (SING), eastern (I39PW and I40PG) and to a certain degree probably even
 370 northeastern directions (I30JP).

371 The given ~~attenuation-transmission loss~~ modeling provides a map-based estimation at surface level
 372 where stratospheric conditions are favorable or unfavorable for infrasound ducting. Complementary
 373 to this, range-dependent propagation modeling is conducted between the epicenter and the four
 374 signal-detecting IMS arrays to estimate the loss of signal amplitude due to atmospheric attenuation as
 375 well as geometric spreading over the considerably large propagation distances of 1800 to 4500 km.
 376 This is performed to estimate if stratospheric propagation is possible, even under weak ducting
 377 conditions or conditions changing with distance.

378 Figure 4 shows tThe atmospheric ducting conditions and corresponding infrasound propagation for the
 379 four stations are shown in figure 4. For I39PW, I07AU and I40PG, stratospheric ducting is modeled in
 380 good agreement with the observed mean celerities of 290, 304 and 309 m/s (see table 1). Following
 381 *Negraru et al. (2010)*, celerities for stratospheric ducting are expected to be in the order of 280 m/s to
 382 320 m/s. Corresponding ray-tracing calculations (not shown here) estimate the celerities of those
 383 stratospheric ducts to be in the order of 290 between 287 m/s and 293 m/s.

384 For I30JP, stratospheric ducting ceases along the 4500 km propagation path due to more unstable
 385 ducting conditions and higher transmission loss (about 150 dB). This is also in good agreement with
 386 the observations, since only a low-frequency signal is recorded at I30JP with a low celerity value of 263
 387 m/s (ray-tracing suggesting 244 m/s), indicative not of a stratospheric but of a thermospheric arrival.



388
 389 *Fig 4: Propagation modeling between the Sulawesi earthquake epicenter (plot origins at 0 km distance)*
 390 *and the infrasound arrays I39PW, I07AU, I40PG and I30JP (respective triangles)*
 391 *using a range-dependent parabolic equation method, quantifying the transmission loss ~~by atmospheric attenuation~~*
 392 *in dB relative to 1 km for a frequency of 1 Hz. ~~An averaged Corresponding~~ effective sound speed profiles*
 393 *(~~v_{eff}~~) ~~are averaged over the complete propagation path~~ is shown for each station.*

394
 395 Thermospheric ducts do not show up in figure 4, since this figure represents a 1 Hz modeling case
 396 highlighting the medium and high frequency stratospheric ducting and resulting in stronger absorption
 397 of thermospheric effects. For lower frequencies in the order of 0.01 Hz to 0.1 Hz, thermospheric
 398 attenuation is considerably small (*Sutherland and Bass, 2004*) and acoustic signal energy can propagate
 399 in the thermospheric duct over large distances with limited transmission loss.

400 ~~The availability of atmospheric ducts can be quantified using. The stability of the ducting conditions are~~
 401 ~~best expressed by quantifying~~ the effective sound speed (v_{eff}) ratio between the stratospheric
 402 maximum (at 40-60 km) and the ground along the propagation path. This parameter indicates
 403 favorable ducting conditions, when being equal or larger than 1 and unfavorable conditions otherwise.
 404 Nevertheless, *Le Pichon et al., 2012* and *Landès et al, 2014* point out that also v_{eff} ratios above 0.9 along
 405 the complete propagation path may lead to at least partially refracted energy in the stratosphere;
 406 whereas this ducting becomes highly likely for values above 0.95. While classical ray-trace modeling
 407 makes a strict separation between ratios larger or smaller than 1 (leading to existing or non-existing

408 stratospheric ducts), the parabolic equation modeling used here also takes into account partial
409 refractions of acoustic energy at effective sound speed ratios near but below 1. ~~This is also a good~~
410 ~~representation of. These partial refractions correspond to~~ small-scale structures like atmospheric
411 gravity waves, ~~which vary~~ing the atmospheric temperature and winds and thus also influencing the
412 infrasound propagation (Kulichkov et al., 2010; Green et al., 2011).

413 The v_{eff} ratios of the average profiles depicted in figure 4 are 0.96 (I39PW), 1.00 (I07AU), 0.99 (I40PG)
414 and 0.93 (I30JP), fully supporting the reasoning above. Not shown in figure 4 are the propagation cases
415 to I06AU and I04AU, having no observations of the event and accordingly low v_{eff} ratios of 0.92 and
416 0.93, while the propagation to the single element station SING is indicative of stratospheric ducting
417 with a higher v_{eff} ratio of 0.98.

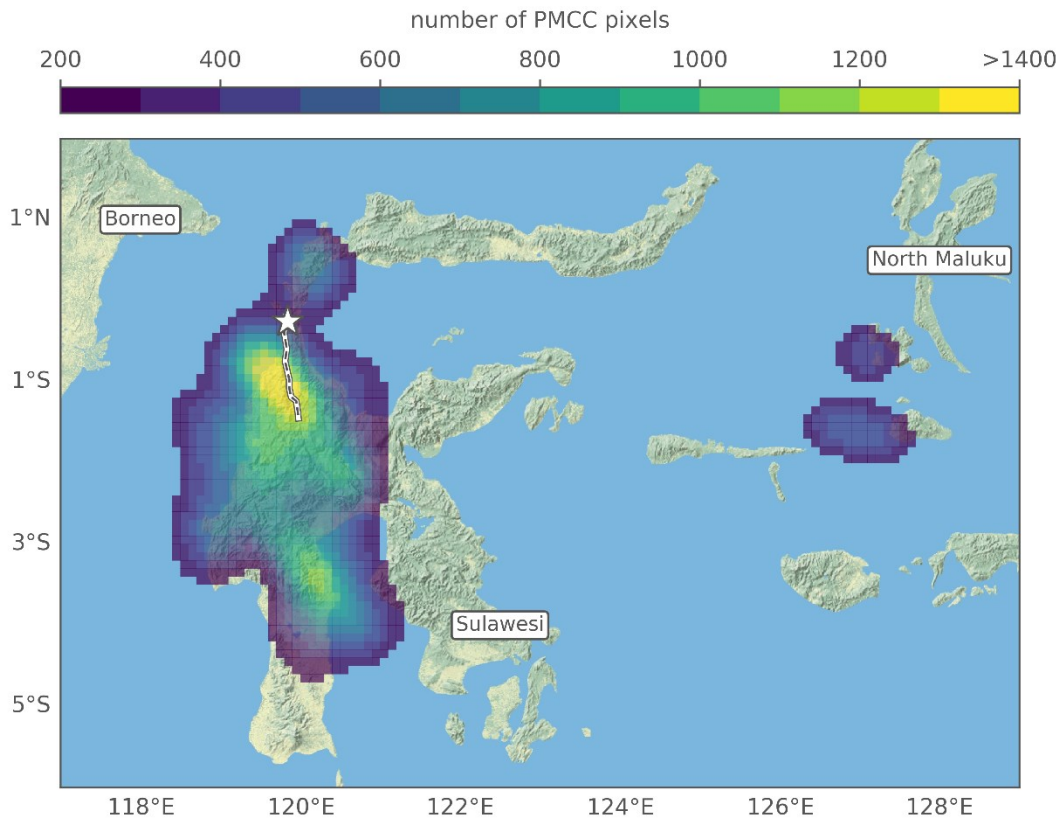
418

419 5. Discussion and Conclusions

420 The main focus of the discussion of observed and modeled signals from the 28th September 2018
421 Sulawesi earthquake is on the source regions and source mechanisms responsible for ~~it~~them. To
422 support this discussion, a ~~back-tracking~~back projection procedure (comparable to the one applied in
423 Shani-Kadmiel et al., 2017 and in the supplement to Gaebler et al., 2019) is applied using the observed
424 PMCC pixels and ~~back-tracking~~projecting them using their temporal and directional information.

425 ~~Figure 5 shows t~~The back_-projection results towards the island of Sulawesi ~~are presented in figure 5~~
426 in terms of an event density map of the pixel-by-pixel information on their most likely origin locations.
427 A total number of about 107,000 pixels is used to derive the picture, ~~combining the back projections~~
428 ~~of all four stations' PMCC recordings towards the epicenter $\pm 40^\circ$ maximum deviation. Single station~~
429 ~~back projections can be found in the supplementary figure S4.~~ Seismic speeds of 4 km/s, resembling
430 the primary propagation of crustal seismic waves, are combined with 0.3 km/s acoustic celerities
431 representing an average value of the station observations. ~~The u~~Uncertainties ~~to the back-projected~~
432 ~~locations as seen by extended contour regions in figure 5 are due to a number of potential influence~~
433 ~~factors. The choice of a fixed seismic speed and fixed acoustic celerity for all pixels instead of individual~~
434 ~~values is supposed to introduce location deviations. of the m~~Measurements and analyses of back-
435 ~~azimuth directions may contain uncertainties due to array configurations and due to crosswind~~
436 ~~influences on the infrasound propagation. as well as the choice of a fixed seismic speed and acoustic~~
437 ~~celerity for all pixels instead of individual values is supposed to introduce an uncertainty to the back-~~
438 ~~projected locations as seen by the extended contour regions in figure 5. The method does not account~~
439 ~~for atmospheric variability (as does the forward propagation approach of figure 4), introducing certain~~
440 ~~location biases.~~ The velocity-averaged back_-projection nevertheless sufficiently emphasizes the major
441 source regions and infrasound generation mechanisms.

442 A region to the south of the epicenter is highlighted (yellow colors representing the highest event
443 density), well corresponding with the earthquake rupture zone along the Palu-Koro fault line. Up to a
444 certain degree, this method also serves as a cross-bearing location procedure, although stations
445 contributing to it are not equally weighted but weighted by the number of pixels used from the
446 respective stations (in this picture, I07AU dominates the back_-projection, since it has the longest and
447 largest record of the event, ~~also see figure S4~~); The location of the highest event density is at 119.6° E,
448 1.0° S, approximately 80 km south of the epicenter and thus half-way along the rupture.



449

450 *Fig 5: Back projection of the combined PMCC detections from I39PW, I07AU, I40PG and I30JP.*
 451 *Considered is each PMCC pixel's back-azimuth as well as a combination of 4 km/s seismic and 0.3 km/s*
 452 *acoustic celerities, resulting in seismic-to-acoustic conversion locations. Color-coded event density for*
 453 *these locations is shown on a 0.1° x 0.1° grid, highlighting regions with more than 200 back-projected*
 454 *pixels per grid node. The epicenter is marked by an asterisk, the rupture zone traced by a dashed line.*

455

456 The figure highlights that infrasound is radiated not only from a distinct, epicentral point source alone,
 457 but from a region extended in north-south directions following the rupture (in fact the event density
 458 values at the epicenter itself are lower than those in the surrounding regions). Secondary peaks apart
 459 from the basin region around the rupture are identified north of the epicenter and in the southern part
 460 of Sulawesi island. The pixels of this southern secondary color peak are mostly related to the early
 461 parts of the main signal recorded at I07AU, while the central and northern color peaks in the figure are
 462 related to signals arriving some minutes later. This corresponds to the 316° to 323° sweep in I07AU
 463 data from south to north, as described in section 3. The two side-maxima separated from the main
 464 signal's colored region are related to the secondary, seismoacoustic signatures described in section 3.
 465 They are derived from a number of I40PG PMCC pixels and point to a region near the North Maluku
 466 islands east of Sulawesi (also see figure S4). Other secondary-side-maxima as e.g. the ones between
 467 Java and east Timor, also mentioned in section 3, are beyond the map borders and not shown here,
 468 but can be found in figure S4.

469 In general, the results observed and visualized by figure 5 point out that an enlarged region, closely
 470 following the rupture and thus also the topography along the fault, generates the acoustic signals
 471 recorded at the remote infrasound sensors. This includes the rupture region itself suffering most from
 472 the earthquake-related ground motionmovement (offsets of up to 7 m horizontal and 2 m dip slip) as
 473 well as an extended basin area around the rupture, enclosed by mountain chains in mostly north-to-
 474 south directions. Mountainous areas are a well-known source of secondary infrasound and

475 seismoacoustic signatures (e.g. *Arrowsmith et al., 2010*), and correspond to the event density maxima
 476 in figure 5: the mountain chains west and east of the Palu-Koro fault as well as the mountain area in
 477 the south of the island with the highest mountains of the Sulawesi island (Mt. Rantemario and Mt.
 478 Rantekombola, both about 3500 m elevation) generate large portions of the recorded signals. The less
 479 prominent but recognizable regions north of the epicenter (Mt. Fuyul Sojol, 3000 m elevation) and on
 480 the Maluku islands (e.g. Mt. Buku Sibela, 2000 m elevation) are also related to topographic peaks. The
 481 most likely source mechanism for the generation of large parts of the **infrasonic and** seismoacoustic
 482 signals is therefore estimated to be the shaking of elevated or exposed topography **near the rupture**
 483 **zone**, stimulated by crustal seismic or surface waves reaching these areas and turning them into
 484 motion.

485 To qualitatively assess if the super shear nature of the given earthquake or the regional prerequisites
 486 (or both) are responsible for the intense and long-lasting infrasound signals observed, the 28th
 487 September 2018 Sulawesi earthquake is compared to three other super shear earthquakes as well as
 488 three other normal shear earthquakes from the same region (Indonesia and Papua New Guinea).
 489 Shallow events between 5 - 30 km depth were chosen with comparably strong magnitudes of Mw >6.5
 490 so that infrasound generation and detection can be expected. Table 23 chronologically lists these six
 491 events and provides an estimation of the emitted and observed infrasound for all of them.

492

493 *Table 23: List of events similar to the 28th September 2018 Sulawesi earthquake, either in their super*
 494 *shear nature or in their regional origin. The separation between “Event detection” / “No Event*
 495 *Detection” “detecting IMS stations” (not necessary a complete list) as well the “source type / signal*
 496 *evaluation” are is an estimations following data analyses performed by authors of this study.*

Event	Detecting-IMS stations	Source type / signal evaluation
Denali , Alaska/USA, 03.11.2002, Mw 7.9, depth 4.9 km	I53US, I10CA	Super shear earthquake , short duration (10 minutes), strong infrasound at I53US (nearby), weak infrasound at I10CA (remote) generated by topography, also seismic arrivals
Sumatra-Andaman , Indonesia, 26.12.2004, Mw 9.3, depth 30 km	I52GB, (others)	Same region, normal shear earthquake , long duration (30 minutes), strong infrasound, also seismic arrivals and secondary sources related to tsunami and tsunami shoreline interaction
Quinghai , China, 13.04.2010, Mw 6.9, depth 17 km	I34MN	Super shear earthquake , short duration (<10 minutes), weak infrasound, no signal at stations in Japan or Russia, no seismic arrivals
Craig , Alaska/USA, 05.01.2013, Mw 7.5, depth 10 km	I53US, (I56US)	Super shear earthquake , short duration (<10 minutes), weak infrasound, I56US signals probably from other source, also seismic arrivals
Porgera , Papua New Guinea, 25.02.2018, Mw 7.5, depth 25.2 km	I06AU, I07AU, I39PW, I40PG	Same region, normal shear earthquake , long duration (20-60 minutes), strong infrasound related to nearby topography, also seismic arrivals
Kokopo , Papua New Guinea, 14.05.2019, Mw 7.5, depth 10 km	I22FR, I39PW, I40PG	Same region, normal shear earthquake , long duration (10-60 minutes), strong infrasound related to nearby topography, also seismic arrivals

<u>Event</u> (with location, time, magnitude, depth)	<u>Source type</u>	<u>Available IMS stations up to 5000 km distance</u>	
		<u>Event Detection</u> (with distance and PMCC-estimated signal duration)	<u>No Event Detection</u> (with distance)
<u>Denali, Alaska/USA, 03.11.2002, Mw 7.9, depth 4.9 km</u>	<u>Super shear earthquake</u>	<u>I53US (156 km, 10 min)</u> <u>I10CA (3358 km, 30 min)</u>	<u>I59US (4919 km)</u>
<u>Sumatra Andaman, Indonesia, 26.12.2004, Mw 9.3, depth 30 km</u>	<u>Same region, normal shear earthquake</u>	<u>I52GB (2852 km, 30 min)</u>	<u>I07AU (4930 km)</u>
<u>Quinghai, China, 13.04.2010, Mw 6.9, depth 17 km</u>	<u>Super shear earthquake</u>	<u>I34MN (1810 km, 10 min)</u>	<u>I46RU (2480 km)</u> <u>I45RU (3273 km)</u> <u>I31KZ (3669 km)</u> <u>I30JP (3996 km)</u> <u>I39PW (4831 km)</u>
<u>Craig, Alaska/USA, 05.01.2013, Mw 7.5, depth 10 km</u>	<u>Super shear earthquake</u>	<u>I53US (1294 km, 5 min)</u> <u>I56US (1443 km, 10 min)</u>	<u>I10CA (2647 km)</u> <u>I57US (2795 km)</u> <u>I18DK (3509 km)</u> <u>I44RU (4236 km)</u> <u>I59US (4334 km)</u>
<u>Porgera, Papua New Guinea, 25.02.2018, Mw 7.5, depth 25.2 km</u>	<u>Same region, normal shear earthquake</u>	<u>I40PG (1044 km, 60 min)</u> <u>I39PW (1759 km, 45 min)</u> <u>I07AU (1784 km, 45 min)</u> <u>I60US (3835 km, 45 min)</u> <u>I04AU (4164 km, 15 min)</u>	<u>I22FR (3144 km)</u> <u>I05AU (4064 km)</u> <u>I30JP (4587 km)</u>
<u>Kokopo, Papua New Guinea, 14.05.2019, Mw 7.5, depth 10 km</u>	<u>Same region, normal shear earthquake</u>	<u>I40PG (72 km, 10 min)</u> <u>I39PW (2379 km, 30 min)</u> <u>I22FR (2527 km, 10 min)</u>	<u>I07AU (2649 km)</u> <u>I60US (3004 km)</u> <u>I05AU (4286 km)</u> <u>I30JP (4542 km)</u> <u>I58US (4803 km)</u>

497

498 The three super shear earthquakes named after ~~Mount the~~ Denali fault, the Quinghai province and the
499 city of Craig, occurring in 2002, 2010 and 2013, are the earthquakes most recent, most intense and
500 most similar in their super shear characteristics to the 28th September 2018 Sulawesi earthquake, also
501 having super shear rupture velocities of 4 to 6 km/s (see Dunham and Archuleta, 2004; Wang and Mori,
502 2012; Yue et al., 2013). Although the IMS infrasound network is not fully established yet (to the time
503 of the Sulawesi earthquake, 80% of the stations were certified and operational, while it were only 8%
504 to the time of the Denali earthquake and about 70% during the time of the other two earthquakes), at
505 least one infrasound array was able to unambiguously detect and characterize each of the mentioned
506 earthquakes.

507 The infrasound signals for Denali earthquake indicate ~~strong infrasound signals~~ a high signal-to-noise
508 ratio at the nearby I53US station as well as a much weaker signals at I10CA in a much larger distance.
509 This event was a good opportunity to track the infrasound back to its generation region in the Alaska
510 Mountain Range along the Denali fault where the rupture occurred (observed in I53US data, *Olsen et*
511 *al., 2003*) and to the Rocky Mountain Chain south-east of it (observed in I10CA data), where similar
512 observations were made for the 1964 Great Alaskan earthquake (see Young and Greene, 1982). The
513 strong movement of local and remote topography generated the infrasound in good agreement with
514 the Sulawesi case. However, no indication is given that the super shear characteristics of the Denali
515 earthquake specially favors the generation of infrasound. For the Quinghai and Craig earthquakes, also
516 reported to be super shear, much weaker and shorter duration infrasound is observed at stations in
517 distances of 1400 km (I53US to Craig) to 1800 km (I34MN to Quinghai), compared to Sulawesi where
518 stronger and much longer infrasound signals were observed between 1800 km and 4500 km. Again,
519 these do not indicate any connection between those previous super shear earthquakes and
520 extraordinary infrasound generation.

521 The Sulawesi earthquake is also compared to three strong earthquakes within the same region, most
522 prominently two nearby Papua New Guinea earthquakes (near the Porgera mine, 2018 and Kokopo
523 city, 2019) of the same magnitude occurring half a year before and after the Sulawesi one, showing
524 ~~strong and~~ clearly observed infrasound signals with high signal-to-noise ratios at multiple IMS stations
525 as well. These infrasound signals are observed up to similar distances as in the Sulawesi case and also
526 provide long-duration, strong amplitude wave energy associated to infrasonic and seismoacoustic
527 arrivals coming from the two earthquakes. Clear seismic signals are also present in the recordings (as
528 in most cases described before, apart from Quinghai) and an association to topographic features as
529 infrasound source regions is possible (the mountain chain in central Papua New Guinea for Porgera
530 and the mountain areas in New Britain and New Ireland for Kokopo). For the Sumatra Andaman
531 earthquake of 2004, strong infrasound with long signal durations was observed and could be back-
532 ~~tracked~~ projected to topographic features of islands and shorelines, especially where the follow-up
533 tsunami reached the shoreline of the Bay of Bengal (see *Le Pichon et al., 2005*). None of the presented
534 earthquakes were super shear earthquakes, but all of them, especially the two very similar Papua New
535 Guinea earthquakes generated strong infrasonic signals comparable to the signals of the Sulawesi
536 event.

537 ~~This leads to the conclusion that from comparison with other events, It can be concluded from~~
538 comparison with other events above that strong infrasound generated by an earthquake is not mainly
539 or exclusively linked to the earthquake's super shear ~~characteristic~~ nature of an earthquake is the most
540 prominent or even exclusive feature linked to strong infrasound generated by an earthquake, but most
541 likely to the nearby existence of mountainous topography. This topography serves as a large-area
542 resonating membrane in terms of large masses brought into motion by a triggering earthquake, ~~which~~
543 ~~then~~ These mass movements produces large amounts of acoustic energy, which can be recorded at
544 nearby or remote infrasound stations given conducive propagation conditions.

545 ~~Since~~ The given super shear event resembles one of only few large magnitude, shallow earthquakes
546 generating pronounced infrasound, ~~it~~ it therefore provides a unique opportunity to study earthquake
547 generated infrasound in terms of the source mechanisms, signal characteristics, propagation
548 conditions and ducting behavior. It also supports the improved understanding of the process of
549 ~~stimulating~~ infrasound radiation by mountain shaking from large earthquakes and the conversion of
550 seismic to acoustic energy.

551 ~~While this study provides the observation analyses and modeling results for the Sulawesi earthquake~~
552 ~~and a qualitative comparison to other events, it cannot provide a comprehensive investigation taking~~

553 ~~into account every detail to utmost precision.~~ Measurement uncertainties within this study are due to
554 the instrumentation and methods applied; modeling uncertainties are due to assumptions applied
555 within the models and due to multi-scale atmospheric variations between source and receivers leading
556 to uncertainties in the ~~attenuation transmission loss~~ and propagation calculations. Taking into account
557 these uncertainties ~~and allows to improve~~ the methods and models to cope with ~~such them issues~~
558 in the future. It will help to gain novel and enhanced insights about infrasound observations and
559 modeling in general and earthquake generated infrasound in particular. This will also help to optimize
560 seismoacoustic observation networks in terms of better understanding the instrumental needs and
561 better evaluating the signatures observable by it. It will finally support seismoacoustic studies of
562 natural as well as anthropogenic infrasound sources in the future and thereby support the infrasound
563 monitoring for treaty verification purposes of the CTBT, as did other CTBT-related studies about
564 infrasound observation, propagation and signal characterization (Assink et al., 2016; Bowman, 2019;
565 Gaebler et al., 2019).

566

567 **Acknowledgements**

568 This work comprises Earth Observatory of Singapore contribution no. 249. This research is partly
569 supported by the National Research Foundation Singapore and the Singapore Ministry of Education
570 under the Research Centres of Excellence initiative.

571

572 **Data availability**

573 Information about earthquake magnitude, location and frequency of occurrence in the region of
574 interest is retrieved from the online-accessible archive of the USGS, see
575 <https://earthquake.usgs.gov/earthquakes/> (last accessed ~~23.02.09.05~~.2019).

576 Atmospheric wind and temperature profiles are derived from ~~the ECMWF~~ operational high-resolution
577 atmospheric model analysis, defined by the Integrated Forecast System of the ECMWF, available at
578 <https://www.ecmwf.int/> (last accessed ~~02.09.23.05~~.2019).

579 Waveform data for the infrasound arrays of the CTBTO IMS (<https://www.ctbto.org/>) used in this study
580 are available to the authors being members of National Data Centers for the CTBTO. Waveform data
581 for SING infrasound station are available to the authors being members of the Earth Observatory of
582 Singapore.

583

584 **Competing Interests**

585 none

586

587 **Author Contributions**

588 **CP** analyzed the waveform data, performed the propagation modeling, wrote the manuscript text and
589 coordinated the co-author contributions; **PG** compiled the data, generated the figures and helped with
590 finalizing the manuscript layout; **LC** provided first ideas and initiated the collaborative study; **ALP**
591 provided expertise in earthquake infrasound, comparison to other events and initiated the
592 collaborative study; **JV** analyzed the waveform data and performed propagation modeling; **AP**
593 analyzed the waveform data and provided manuscript text; **DT** performed the attenuation modeling

594 and provided manuscript text; **BT** provided first ideas and initiated the collaborative study; **all authors**
595 supported and improved the draft by proof-reading, commenting or correcting the manuscript.

596

597 **References**

598 [Ardhuin, F. and Herbers, T.H.C.: Noise generation in the solid Earth, oceans and atmosphere, from](#)
599 [nonlinear interacting surface gravity waves in finite depth, *Journal of Fluid Mechanics*, 716, doi:](#)
600 [10.1017/jfm.2012.548, 2013.](#)

601 Arrowsmith, S.J., Johnson, J.B., Drob, D.P., and Hedlin, M.A.H.: The seismoacoustic wavefield: A new
602 paradigm in studying geophysical phenomena, *Review of Geophysics*, 48, doi:
603 10.1029/2010RG000335, 2010.

604 [Assink, J. D., Averbuch, G., Smets, P. S. M., and Evers, L. G.: On the infrasound detected from the 2013](#)
605 [and 2016 DPRK's underground nuclear tests, *Geophysical Research Letters*, 43, doi:](#)
606 [10.1002/2016GL068497, 2016.](#)

607 Bao, H., Ampuero, J.-P., Meng, L., Fielding, E.J., Liang, C., Milliner, C.W.D., Feng, T., and Huang, H.: Early
608 and persistent supershear rupture of the 2018 magnitude 7.5 Palu earthquake, *Nature Geoscience*, 12,
609 doi: 10.1038/s41561-018-0297-z, 2019.

610 [Bernard, P. and Baumont, D.: Shear Mach wave characterization for kinematic fault rupture models](#)
611 [with constant supershear rupture velocity, *Geophysical Journal International*, 162 doi: 10.1111/j.1365-](#)
612 [246X.2005.02611.x, 2005.](#)

613 Bouchon, M., Toksöz, N., Karabulut, H., Bouin, M.-P., Dietrich, M., Aktar, M., and Edie, M.: Seismic
614 imaging of the 1999 Izmit (Turkey) Rupture inferred from the near-fault recordings, *Geophysical*
615 *Research Letters*, 27, doi: 10.1029/2000GL011761, 2000.

616 Bouchon, M. and Vallée, M.: Observation of Long Supershear Rupture during the Magnitude 8.1
617 Kunlunshan Earthquake, *Science*, 301, doi: 10.1126/science.1086832, 2003.

618 [Bowman, D. C.: Yield and emplacement depth effects on acoustic signals from buried explosions in](#)
619 [hard rock, *Bulletin of the Seismological Society of America*, 109, doi: 10.1785/0120180285, 2019.](#)

620 Cansi, Y.: An automatic seismic event processing for detection and location: the PMCC method,
621 *Geophysical Research Letters*, 22, doi: 10.1029/95GL00468, 1995.

622 [Doan, M.-L. and Gary, G., Rock pulverization at high strain rate near the San Andreas fault, *Nature*](#)
623 [*Geosciences*, 2, doi: 10.1038/NGEO640, 2009.](#)

624 [Donn, W.L. and Naini, B.: Sea wave origin of microbaroms and microseisms, *Journal of Geophysical*](#)
625 [*Research*, 78, doi: 10.1029/JC078i021p04482, 1973.](#)

626 Drob, D. P., Picone, J. M., and Garcés, M. A.: Global morphology of infrasound propagation, *Journal of*
627 *Geophysical Research*, 108, doi: 10.1029/2002JD003307, 2003.

628 Drob, D. P., Emmert, J. T., Crowley, G., Picone, J. M., Shepherd, G. G., Skinner, W., Hays, P., Niciejewski,
629 R. J., Larsen, M., She, C. Y., Meriwether, J. W., Hernandez, G., Jarvis, M. J., Sipler, D. P., Tepley, C. A.,
630 O'Brien, M. S., Bowman, J. R., Wu, Q., Murayama, Y., Kawamura, S., Reid, I. M., and Vincent R. A.: An
631 Empirical Model of the Earth's Horizontal Wind Fields: HWM07, *Journal of Geophysical Research*, 113,
632 doi: 10.1029/2008JA013668, 2008.

633 Dunham, E.M. and Archuleta, R. J.: Evidence for a Supershear Transient during the 2002 Denali Fault
634 Earthquake, *Bulletin of the Seismological Society of America*, 94, doi: 10.1785/0120040616, 2004.

635 Gaebler, P., Ceranna, L., Nooshiri, N., Barth, A., Cesca, S., Frei, M., Grünberg, I., Hartmann, G., Koch, K.,
636 Pilger, C., Ross, J. O., and Dahm, T.: A multi-technology analysis of the 2017 North Korean nuclear test,
637 *Solid Earth*, 10, doi: 10.5194/se-10-59-2019, 2019.

638 Garcés, M. A.: On Infrasound Standards, Part 1: Time, Frequency, and Energy Scaling, *InfraMatics* 2,
639 doi: 10.4236/inframatics.2013.22002, 2013.

640 Gibbons, S. J., Asming, V., Eliasson, L., Fedorov, A., Fyen, J., Kero, J., Kozlovskaya, E., Kvaerna, T., Liszka,
641 L., Näsholm, S. P., Raita, T., Roth, M., Tiira, T., and Vinogradov, Y.: The European Arctic: A Laboratory
642 for Seismoacoustic Studies, *Seismological Research Letters*, 86, doi: 10.1785/0220140230, 2015a.

643 Gibbons, S. J., Kvaerna, T., and Mykkeltveit, S.: Could the IMS Infrasound Stations Support a Global
644 Network of Small Aperture Seismic Arrays?, *Seismological Research Letters*, 86, doi:
645 10.1785/0220150068, 2015b.

646 Green, D.N., Vergoz, J., Gibson, R., Le Pichon A., and Ceranna, L.: Infrasound radiated by the Gerdec
647 and Chelopechene explosions: propagation along unexpected paths, *Geophysical Journal
648 International*, 185, doi: 10.1111/j.1365-246X.2011.04975.x, 2011.

649 Hedlin, M.A.H., Walker, K. T., Drob, D. P., and de Groot-Hedlin, C. D.: Infrasound: Connecting the Solid
650 Earth, Oceans, and Atmosphere, *Annual Review of Earth and Planetary Sciences*, 40, doi:
651 10.1146/annurev-earth-042711-105508, 2012.

652 Heidarzadeh, M., Muhari, A., and Wijanarto, A.B.: Insights on the Source of the 28 September 2018
653 Sulawesi Tsunami, Indonesia Based on Spectral Analyses and Numerical Simulations, *Pure and Applied
654 Geophysics*, 176, doi: 10.1007/s00024-018-2065-9, 2019.

655 Hernandez, B., Le Pichon, A., Vergoz, J., Herry, P., Ceranna, L., Pilger, C., Marchetti, E., Ripepe, M., and
656 Bossu, R.: Estimating the Ground-Motion Distribution of the 2016 Mw 6.2 Amatrice, Italy, Earthquake
657 Using Remote Infrasound Observations, *Seismological Research Letters*, 89, doi: 10.1785/0220180103,
658 2018.

659 [Jamelot, A., Gailler, A., Heinrich, P., Vallage, A., and Champenois, J.: Tsunami Simulations of the](#)
660 [Sulawesi Mw 7.5 Event: Comparison of Seismic Sources Issued from a Tsunami Warning Context Versus](#)
661 [Post-Event Finite Source, *Pure and Applied Geophysics*, 176, doi: 10.1007/s00024-019-02274-5, 2019.](#)

662 Katili, J. A.: Past and Present Geotectonic Position of Sulawesi, Indonesia, *Tectonophysics*, 45, doi:
663 10.1016/0040-1951(78)90166-X, 1978.

664 Kulichkov, S.N., Chunchuzov, I. P., and Popov, O. I.: Simulating the Influence of an Atmospheric Fine
665 Inhomogeneous Structure on Long Range Propagation of Pulsed Acoustic Signals, *Izvestiya
666 Atmospheric and Oceanic Physics*, 46, doi: 10.1134/S0001433810010093, 2010.

667 Landès, M., Le Pichon, A., Shapiro, N.M., Hillers, G., and Campillo, M.: Explaining global patterns of
668 microbarom observations with wave action models, *Geophysical Journal International*, 199, doi:
669 10.1093/gji/ggu324, 2014.

670 Le Pichon, A., Guilbert, J., Vega, A., Garcés, M. A., and Brachet, N.: Ground-coupled air waves and
671 diffracted infrasound from the Arequipa earthquake of June 23, 2001, *Geophysical Research Letters*,
672 29, doi: 10.1029/2002GL015052, 2002.

673 Le Pichon, A., Guilbert, J., Vallée, M., Dessa, J. X., and Ulziibat, M.: Infrasonic imaging of the Kunlun
674 Mountains for the great 2001 China earthquake, *Geophysical Research Letters*, 30, doi:
675 10.1029/2003GL017581, 2003.

676 Le Pichon, A., Herry, P., Mialle, P., Vergoz, J., Brachet, N., Garces, M. A., Drob, D., and Ceranna, L.:
677 Infrasonic associated with 2004-2005 large Sumatra earthquakes and tsunami, *Geophysical Research*
678 *Letters*, 32, doi: 10.1029/2005GL023893, 2005.

679 Le Pichon, A., Mialle, P., Guilbert, J., and Vergoz, J.: Multistation infrasonic observations of the Chilean
680 earthquake of 2005 June 13, *Geophysical Journal International*, 167, doi: 10.1111/j.1365-
681 246X.2006.03190.x, 2006.

682 Le Pichon, A., Blanc, E., and Hauchecorne, A. (Eds.): *Infrasound Monitoring for Atmospheric Studies*,
683 Springer, ISBN: 978-1-4020-9507-8, 2010.

684 Le Pichon, A., Ceranna, L., and Vergoz, J.: Incorporating numerical modeling into estimates of the
685 detection capability of the IMS infrasonic network, *Journal of Geophysical Research*, 117, doi:
686 10.1029/2011JD016670, 2012.

687 Le Pichon, A., Blanc, E., and Hauchecorne, A. (Eds.): *Infrasound for Atmospheric Studies – Challenges*
688 *in Middle Atmosphere Dynamics and Societal Benefits*, Springer, ISBN: 978-3-319-75138-2, 2019.

689 Marchetti, E., Lacanna, G., Le Pichon, A., Piccinini, D., and Ripepe, M.: Evidence of large infrasonic
690 radiation induced by earthquake interaction with alluvial sediments, *Seismological Research Letters*,
691 87, doi: 10.1785/0220150223, 2016.

692 [Matoza, R., Green, D. N., Le Pichon, A., Shearer, P. M., Fee, D., Mialle, P., and Ceranna, L.: Automated](#)
693 [detection and cataloging of global explosive volcanism using the International Monitoring System](#)
694 [infrasonic network, *Journal of Geophysical Research Solid Earth*, 122, doi: 10.1002/2016JB013356,](#)
695 [2017.](#)

696 Mutschlecner, J. P. and Whitaker, R. W.: Infrasonic from earthquakes, *Journal of Geophysical*
697 *Research*, 110, doi: 10.1029/2004JD005067, 2005.

698 Negru, P. T., Golden, P., and Herrin, E.T.: Infrasonic Propagation in the “Zone of Silence”,
699 *Seismological Research Letters*, 81, doi: 10.1785/gssrl.81.4.615, 2010.

700 Olson, J.V., Wilson, C.R., and Hansen, R.A.: Infrasonic associated with the 2002 Denali fault
701 earthquake, Alaska, *Geophysical Research Letters*, doi: 10.1029/2003GL018568, 2003.

702 Omira, R., Dogan, G. G., Hidayat, R., Husrin, S., Prasetya, G., Annunziato, A., Proietti, C., Probst, P.,
703 Paparo, M. A., Wronna, M., Zaytsev, A., Pronin, P., Giniyatullin, A., Putra, P. S., Hartanto, D., Ginanjar,
704 G., Kongko, W., Pelinovsky, E., and Yalciner, A. C.: The September 28th, 2018, Tsunami In Palu-Sulawesi,
705 Indonesia: A Post-Event Field Survey, *Pure and Applied Geophysics* 176, doi: 10.1007/s00024-019-
706 02145-z, 2019.

707 Pailoplee, S.: Probabilities of Earthquake Occurrences along the Sumatra-Andaman Subduction Zone,
708 *Open Geosciences*, 9, doi: 10.1515/geo-2017-0004, 2017.

709 Picone, J. M., Hedin, A. E., Drob, D. P., and Aikin, A. C.: NRLMSISE-00 Empirical Model of the
710 Atmosphere: Statistical Comparisons and Scientific Issues, *Journal of Geophysical Research*, 107, doi:
711 10.1029/2002JA009430, 2002.

712 Pilger, C., Ceranna, L., Ross, J.O., Vergoz, J., Le Pichon, A., Brachet, N., Blanc, E., Kero, J., Liszka, L.,
713 Gibbons, S., Kvaerna, T., Näsholm, S.P., Marchetti, E., Ripepe, M., Smets, P., Evers, L., Ghica, D., Ionescu,

- 714 C., Sindelarova, T., Ben Horin, Y., and P. Mialle: The European Infrasound Bulletin, Pure and Applied
715 Geophysics, 175, doi: 10.1007/s00024-018-1900-3, 2018.
- 716 Shani-Kadmiel, S., Assink, J.D., Smets, P.S.M., and Evers, L.G.: Seismoacoustic coupled signals from
717 earthquakes in Central Italy: epicentral and secondary sources of infrasound, Geophysical Research
718 Letters, 45, doi: 10.1002/2017GL076125, 2017.
- 719 Socquet, A., Hollingsworth, J., Pathier, E., and Bouchon, M.: Evidence of supershear during the 2018
720 magnitude 7.5 Palu earthquake from space geodesy, Nature Geosciences, 12, doi: 10.1038/s41561-
721 018-0296-0, 2019.
- 722 Sutherland, L. C. and Bass, H. E.: Atmospheric absorption in the atmosphere up to 160 km, Journal of
723 the Acoustical Society of America, 115, doi: 10.1121/1.1631937, 2004.
- 724 Tailpied, D., Le Pichon, A., Marchetti, E., Assink, J., and Vergnolle, S.: Assessing and optimizing the
725 performance of infrasound networks to monitor volcanic eruptions, Geophysical
726 Journal International, 208, doi: 10.1093/gji/ggw400, 2017.
- 727 [USGS: U.S. Geological Survey, Sulawesi 2018 earthquake event page, available at:](https://earthquake.usgs.gov/earthquakes/eventpage/us1000h3p4/)
728 <https://earthquake.usgs.gov/earthquakes/eventpage/us1000h3p4/> (last accessed 02.09.2019), 2018.
- 729 [Walker, K. T., Le Pichon, A., Kim, T. S., de Groot-Hedlin, C., Che, I.-Y., and Garcés, M.: An analysis of](#)
730 [ground shaking and transmission loss from infrasound generated by the 2011 Tohoku earthquake,](#)
731 [Journal of Geophysical Research, 118, doi: 10.1002/2013JD020187, 2013.](#)
- 732 Wang, D. and Mori, J.: The 2010 Qinghai, China, Earthquake: A Moderate Earthquake with Supershear
733 Rupture, Bulletin of the Seismological Society of America, 102, doi: 10.1785/0120110034, 2012.
- 734 Waxler, R., Assink, J., Hetzer, C., and Velea, D.: NCPAprop – A software package for infrasound
735 propagation modeling, Journal of the Acoustical Society of America, 141, doi: 10.1121/1.4987797,
736 2017.
- 737 Wilson, D. K.: The sound-speed gradient and refraction in the near-ground atmosphere, Journal of the
738 Acoustical Society of America, 113, doi: 10.1121/1.1532028, 2003.
- 739 [Young, J. M. and Greene, G. E.: Anomalous infrasound generated by the Alaskan earthquake of 28](#)
740 [march 1964, Journal of the Acoustical Society of America, 71, doi: 10.1121/1.387457, 1982.](#)
- 741 Yue, H., Lay, T., Freymueller, J. T., Ding, K., Rivera, L., Ruppert, N. A., and Koper, K. D.: Supershear
742 rupture of the 5 January 2013 Craig, Alaska (Mw 7.5) earthquake, Journal of Geophysical Research, doi:
743 10.1002/2013JB010594, 2013.

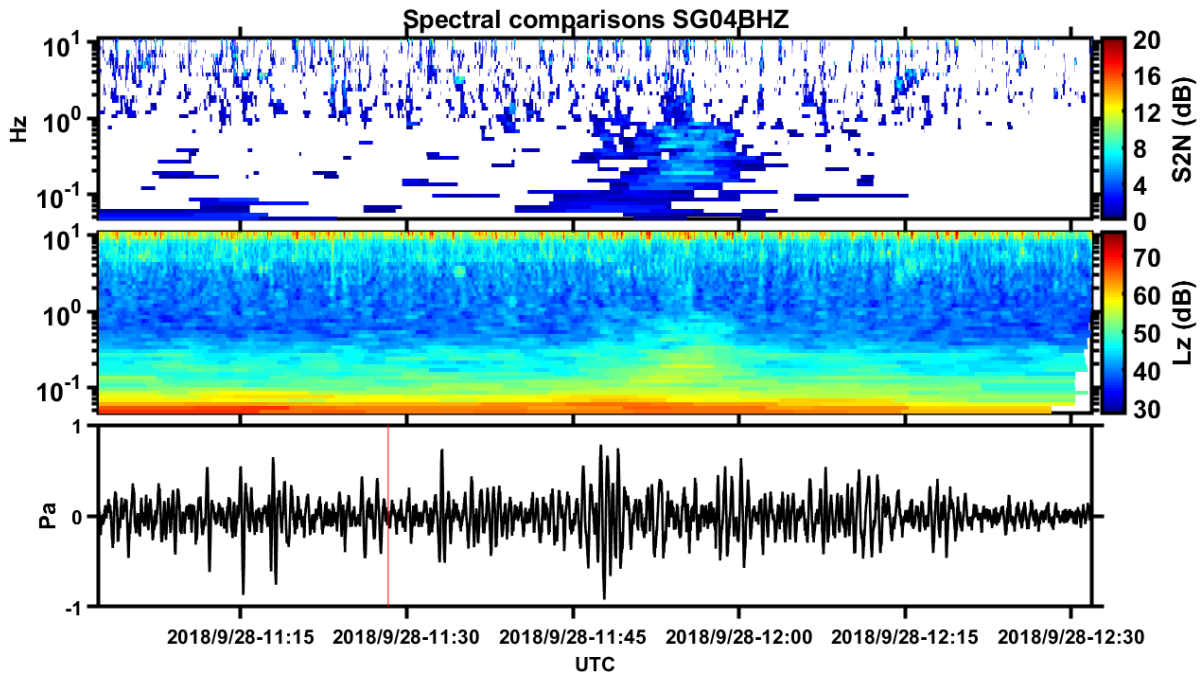
744

745 Supplementary Material

746

747 Figure S1

748

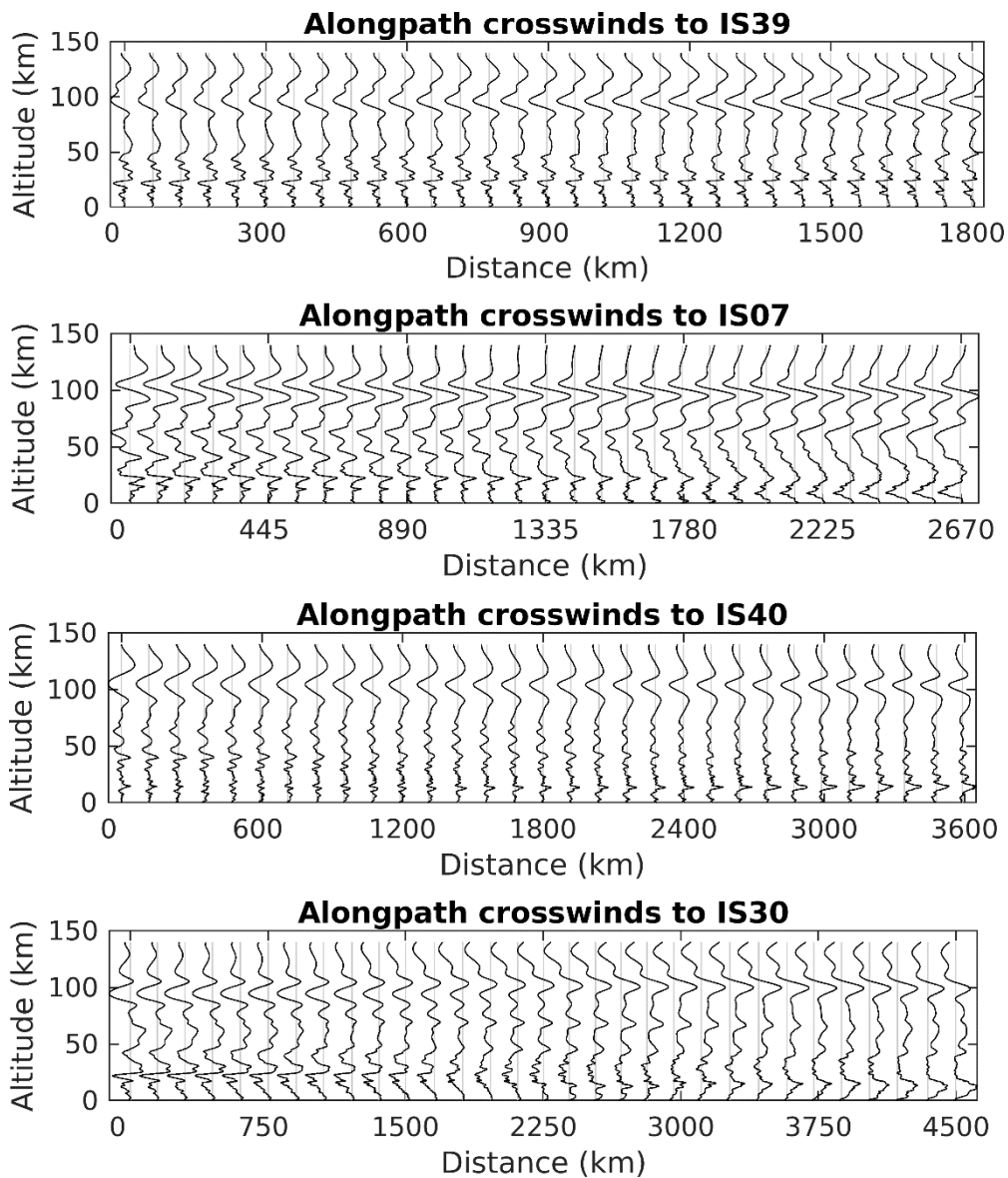


749

750 *Fig S1: Example of INFERNO analysis for the Singapore station (SING). The bottom panel is the*
751 *waveform recorded at sensor SG04, with the red vertical line representing an estimated arrival time*
752 *based on the location and time of the earthquake. The middle panel is an example of an INFERNO*
753 *spectrogram where energy is calculated in fractional octave bands. The top panel is a signal to noise*
754 *plot derived from the spectrogram. All the values for each frequency band are averaged and a 3dB*
755 *threshold is set. Note that while the signal from the event is not as obvious within the waveform and*
756 *spectrogram, the signal to noise plot clearly shows the signals arrival.*

757 **Figure S2**

758

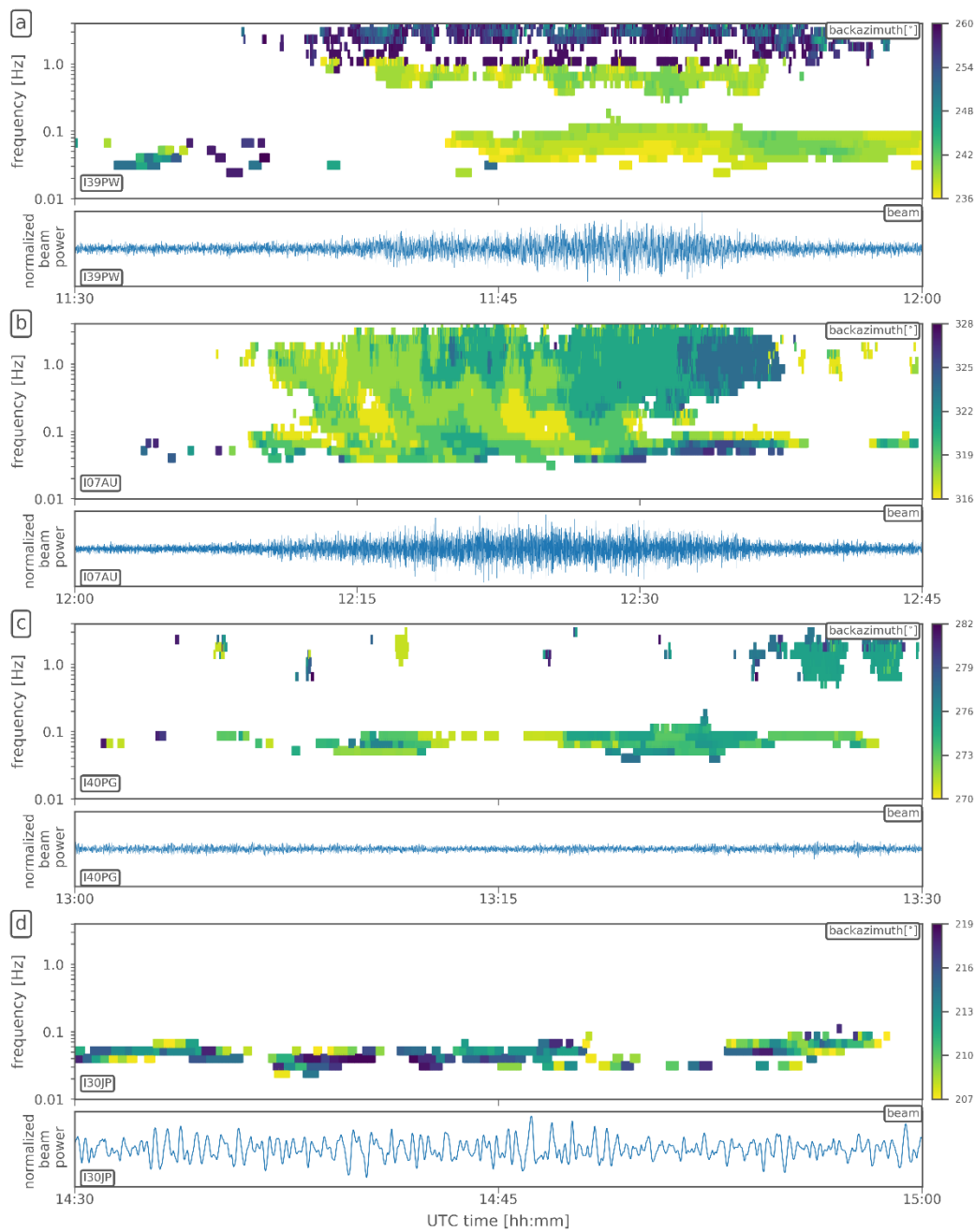


759

760 *Fig S2: Crosswind profiles along the propagation path from the epicenter to the four arrays. Positive*
761 *values correspond to winds in the 90° clockwise perpendicular direction, the distance between two*
762 *vertical lines corresponds to 50 m/s wind intensity. Range-dependent ECMWF profiles merged with*
763 *climatologies are used as described in the data section. Enhanced positive crosswinds potentially*
764 *responsible for positive back-azimuth deviations occur at I39PW around the stratospheric turning*
765 *altitude of 50 km and to some degree below that altitude. Strong negative crosswinds at 50 km altitude*
766 *and below occur at I07AU and might explain negative back-azimuth deviations for this station. Weak*
767 *total crosswinds at and below 50 km at station I40PG might explain marginal back-azimuth deviations*
768 *at this station. Strong thermospheric crosswinds around 100 km and below might explain back-azimuth*
769 *deviations at I30JP after thermospheric propagation.*

770 **Figure S3**

771



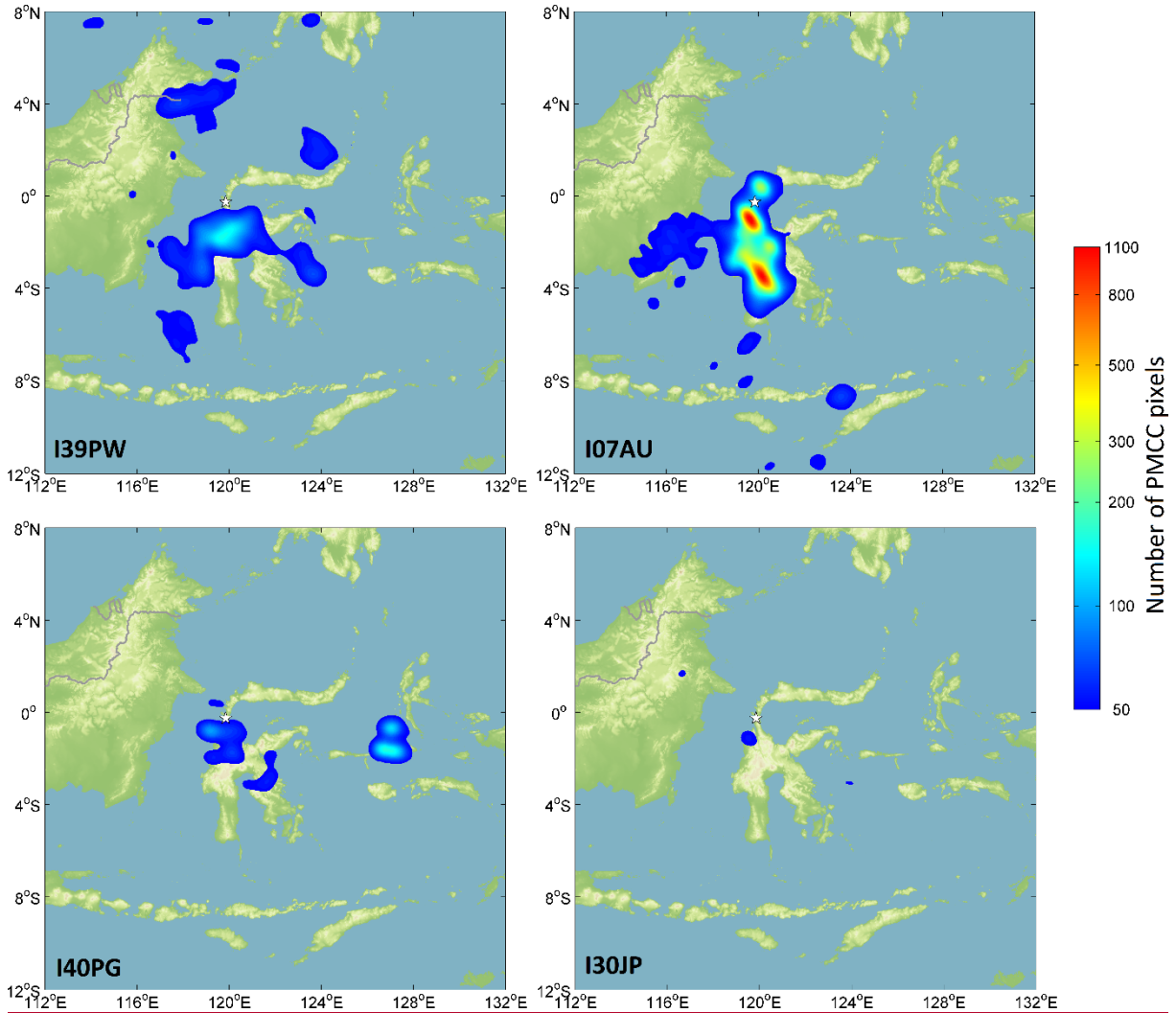
772

773 *Fig S3: Waveform beams and PMCC backazimuth information for the four infrasound arrays of figure*
774 *2. Absolute backazimuth directions are provided here instead of epicentral deviations, allowing to*
775 *quantify changes and differences in the direction of signal origin. A small azimuthal section ($\pm 12^\circ$ from*
776 *the expected epicenter direction in subfigure a, $\pm 6^\circ$ in subfigure b, c and d) and short time window (30*
777 *min in subfigures a, c and d, 45 min in subfigure b) is chosen to highlight the epicentral infrasound's*
778 *origin direction and arrival time as specified in table 1. Differences in the direction of origin between*
779 *the high-frequency and the mid- to low-frequency parts of the epicentral infrasound are found at I39PW*
780 *(subfigure a) in the order of $\pm 10^\circ$. An azimuthal sweep of about 7° is observed at I07AU (subfigure b).*
781 *Both phenomena indicate a spatially and temporally extended source. Only small and mostly arbitrary*
782 *backazimuth variation is present at stations I40PG and I30JP (subfigures c and d).*

783

Figure S4

784



785

786

787 *Fig S4: Single-station back projection maps for the four infrasound arrays. The colorbar of each figure*
 788 *starts at a 4 time lower value than in the cumulative 4-station-figure 5. The main region near the*
 789 *epicenter (marked by a star) and the rupture south of it are projected reasonably well for each station.*
 790 *The directional deviation and spatial extension of the back-projected source regions per station*
 791 *corresponds to backazimuth variations as e.g. the azimuthal sweep in figure S3. Additionally, regions*
 792 *of potential seismoacoustic signal generation are identified around the island of Sulawesi, as described*
 793 *in the manuscript text.*